AGARD

ADVISORY GROUP FOR AEROSPACE RESEARCH & DEVELOPMENT

7 RUE ANCELLE 92200 NEUILLY SUR SEINE FRANCE

Paper Reprinted from
Conference Proceedings No. 301

AERODYNAMICS OF POWER PLANT INSTALLATION

NORTH ATLANTIC TREATY ORGANIZATION

AIRFRAME-PROPULSION SYSTEM AERODYNAMIC INTERFERENCE PREDICTIONS AT HIGH TRANSONIC MACH NUMBERS INCLUDING OFF-DESIGN ENGINE AIRFLOW EFFECTS

by
*R. M. Kulfan and **A. Sigalla
Boeing Commercial Airplane Company
P.O. Box 3707
Seattle, Washington 98124
USA

SUMMARY

Flow interference between engine nacelles and an airframe has an important effect on the aerodynamic efficiency of all types of aircraft. The performance of airplanes designed for supersonic flight particularly has been affected by adverse interference forces. This has been the case most often at transonic speeds.

This paper emphasizes the transonic speed regime for airplanes at conditions where inlet spillage takes place. Relatively recent availability of appropriate wind tunnel data has now made it possible to assess available theoretical methods.

The National Aeronautics and Space Administration, NASA, conducted an extensive wind-tunnel test program to evaluate aerodynamic performance penalties associated with propulsion system installation and operation at subsonic through low supersonic speeds. Using those test data, a study to assess the accuracy of analytic methods for predicting transonic engine-airframe interference effects was conducted and forms the content of the paper. Study variables included Mach number, angle of attack, relative nacelle location, and nacelle mass-flow ratio.

Study results included test-theory comparisons of forces as well as induced pressure fields. Prediction capability of induced shock wave strength and locations was assessed. It was found that large interference forces due to engine location and flow spillage occur at transonic speeds; that theory can explain these effects; and that theory, under appropriate conditions, can predict quantitatively these effects.

---

* Senior Specialist Engineer
** Technology Chief—New Product Development

INTRODUCTION

Flow interference between engine nacelles and the airframe has an important effect on the aerodynamic efficiency of all types of aircraft. The performance of airplanes designed for supersonic flight particularly has been affected by adverse mutual interference forces. This has been the case most often at transonic speeds. These adverse effects often have come as a surprise, being discovered in the course of flight testing at a stage in an airplane program when it was too late to do much about the problem. The reasons for this have been: (1) absence of theoretical methods to help the designer in definition of a configuration that would not exhibit such problems, and (2) difficulty of conducting valid experiments that would warn the designer of potential problems.

Theoretical methods and research testing on this subject, in the past, have focused on the supersonic regime of Mach numbers greater than 1.8. This was primarily because theory was easier to develop for that speed regime, and the testing to verify and enhance the theory was simpler to conduct. Beyond that, and more importantly, engine operation for airplanes designed in that flight regime is such that the flow at the engine nacelle inlet lip is more regular; that is, the mass-flow ratio is near unity. At transonic speeds, theory is more difficult, testing more complicated, and the mass-flow ratios of typical propulsion systems are such that significant spillage takes place. Some of the aerodynamic effects of spillage have been difficult to estimate.

This paper emphasizes the transonic speed regime specifically at conditions where inlet spillage takes place. Availability of appropriate wind-tunnel data has now made it possible to realistically assess available theoretical methods. The aim of the paper is to show how these methods compare with experiment.

The National Aeronautics and Space Administration, NASA, has conducted an extensive wind-tunnel test program to evaluate aerodynamic performance penalties associated with propulsion system installation and operation at subsonic through low supersonic speeds. With these test data in hand, a study to assess the accuracy of analytic methods for predicting transonic engine-airframe interference effects was conducted and forms the contents of this paper.

The wind-tunnel model used to obtain the majority of test data reviewed in this paper is described in section 2. Appropriate information on the experimental conditions is given. A brief description of the theoretical methods that were used for comparison with the experimental data is presented in section 3. Obvious limitations of these methods are listed. Systematic comparisons of theory with experiment are shown in section 4. These comparisons include—

- Isolated wing-body lift, drag, and pitching moment
- Isolated nacelle drag and pressure distributions
- Mutual nacelle interference drag for various nacelle arrangements
- Nacelle interference shock-wave patterns and pressure distributions on the wing lower surface
- Total installed nacelle interference effects on lift, drag, and pitching moments
- Certain jet exhaust effects

Discussion of results is included with these comparisons. A general assessment of the paper, together with suggestions for further work, is summarized in section 5.

2.0 MODEL GEOMETRY AND TEST CONDITIONS

The NASA experimental nacelle-airframe interference program was conducted in the Ames 11- by 11-ft wind tunnel. The wind-tunnel model is shown in figure 1. Basic features and details of the model are summarized in figures 2 and 3.

The wing-body configuration is a 0.024-scale model of the U.S. 1971 SST. The wing-body was sting mounted with a six-component internal strain-gage balance. The left-hand wing had 126 static pressure orifices, 95 on the lower surface and 31 on the upper surface. Two different nacelle geometries were tested. One set of nacelles had sharp inlets, and the second set of nacelles had a slightly blunt inlet lip shape. Investigations reported in this paper concern only the sharp-lip nacelles.

The four individual nacelles were supported just below the wing-body model on individual flow-through stings. The two left-hand nacelles were mounted individually on separate six-component internal strain-gage balances. The pressure instrumented nacelles had 40 static-pressure orifices. The six-component force balances used to support the right-hand nacelles were housed in the thickness of each nacelle. A two-shell flow-through balance, located in each nacelle, used four instrumented flexures located 90 deg apart at two axial locations. The nacelle balances measured the aerodynamic forces on the external surface of the nacelle, plus the forces on a small portion of the internal duct near the inlet. The wind-tunnel data corrections included removal of the estimated skin friction drag on this internal duct area.

The nacelle support system could position the nacelles vertically, streamwise, and spanwise, relative to the wing-body combination and to each other. The range of achievable nacelle locations is indicated in figure 2. Staggered and nonstaggered arrangements were tested at six different nacelle stations and three different spanwise locations, as shown in figure 4. The support system also provided for independent control and measurement of mass flow through each nacelle by means of a mass-flow control plug and appropriate pressure instrumentation.

Test conditions included:

- Mach numbers: 0.90, 0.98, 1.1, 1.15, 1.2, 1.3, 1.4
- Angle of attack: α = 0 to 6 deg
- Mass-flow ratio: MFR = 0.6 to 1.0

Test configurations included:

- Isolated wing-body
- Isolated nacelle
- Four nacelles in various relative positions
- Wing-body plus nacelles in various locations

These tested configurations provided the following measurements of isolated and interference data:

- Isolated wing-body data: measurements on wing-body without the nacelles present
- Isolated nacelle data: measurements on a single nacelle
- Mutual nacelle interference: differences in nacelle measurements with and without the other nacelles being present
- Wing-body interference on the nacelles: differences in nacelle measurements with and without the wing-body being present

- Total wing-body plus nacelle data: sum of wing-body data plus nacelle data
- Spillage interference: differences in measurements on identical configurations with the nacelles spilling according to a specific controlled mass-flow ratio (MFR), and the corresponding data obtained without spillage.

The basic force and pressure data are contained in references 1 and 2, respectively. Complete descriptions of the wind-tunnel model, test conditions, and available test data are given in reference 3.

3.0 DISCUSSION OF THEORETICAL METHODS

This paper shows comparisons of theory with experiment and thus provides a basis for assessment of the value of the theory. A discussion of the theoretical methods used for these comparisons is presented in this section.

3.1 Requirements for Formulation of Theory

The objective is to calculate interference forces and flow fields that occur when engine nacelles are located in proximity to other airplane components. This is to be done at high transonic Mach numbers; that is, from just above Mach 1 to approximately Mach 1.4.

To achieve this objective, the minimum requirements for theory must include:

- Ability to predict the flow field around airplane components in terms of changes in pressures and velocities
- Ability to sum the effects of the various flow field components upon one another
- Ability to predict occurrence of shock waves, their propagation, and their strength in order to determine the consequences of shock-wave-induced forces at transonic Mach numbers

It was desired to assess the effects of engine inlet spillage and jet exhaust plume shape upon interference. An additional requirement for the theory was, therefore, prediction of the flow field around an engine nacelle when either the mass-flow ratio into the inlet was less than unity or when the exhaust jet was not fully expanded.

3.2 Theoretical Methods Used in This Paper

The simplest method that meets some of the above requirements is linear small-perturbation theory for supersonic flow. This method has been developed for the calculation of flow fields around airplane components and has been computerized in many versions. With this method, a study configuration can be broken down into its basic components (and also into volume and lifting elements) so that the relative flow influences of all these elements can be examined individually. References 4 through 6 describe some of these computerized versions of linear small-perturbation theory.

Small-perturbation theory cannot be used, however, to predict the occurrence, propagation, and location of shock waves. Thus, it could not by itself be used to meet the third of the above objectives. A modified form of linear theory that can predict the occurrence and location of shock waves around bodies of revolution was therefore used for the force and moment predictions reported in this paper. This method is described in reference 7. Figure 5 illustrates a typical geometrical representation of a wing-body-nacelle configuration for this modified linear theory program.

The flow around a nacelle at mass-flow ratio less than unity with normal shock spillage contains regions of both subsonic and supersonic flow. Small-perturbation theory, even when modified as in reference 7, cannot predict such flows. Because of this, a more complicated method had to be used for the calculation of the nacelle flow fields at spillage conditions. The method used here is a time marching solution of the Euler equations for two-dimensional or axisymmetric flow. The procedure can compute mixed regions of subsonic and supersonic flow and yield shock wave locations as part of the solution. The method, which was coded for computer use, is described in reference 8.

3.3 Limitations of the Theoretical Methods

In general terms, small-perturbation theory is limited to airplane configurations that are thin and slender. Supersonic small-perturbation theory is also limited to flows that do not contain zones of subsonic flow embedded in supersonic flow.

In practical terms, it is useful to categorize limitations of the theory used in this paper as follows:

- Limitations because of viscosity
- Limitations because of mixed subsonic-supersonic flow
- Limitations because of geometry

The first limitation applies when the actual flow is substantially different from the assumed theoretical attached flow conditions because of large areas of flow separation, vortices, wakes, etc. Criteria can be applied to theoretical predictions, which can tell in advance if occurrence of the above has a high degree of probability. Such criteria, based on experiment, have been presented and discussed in reference 9. An application of these criteria to the type of flow discussed in this paper is shown in section 4.3.

As has been mentioned above, the theory based on solution of the Euler equations can account for mixed subsonic-supersonic flow regions in the vicinity of the nacelles, particularly when normal shock spillage takes place. It was not found feasible, for this study, to allow for mixed subsonic-supersonic flows on other parts of the airplane. It was believed, however, that this limitation would affect predictions primarily in the narrow (but not unimportant) Mach range of 0.95 to 1.05. In general, strong shock waves with downstream subsonic flow will also have an adverse effect on boundary layers and limit theory for the viscous reasons already mentioned.

The small-perturbation theory that has been used here is strictly applicable to all wing-body geometries within the above limitations. Calculation of shock waves and mixed-flowfields is applicable, however, only to nacelle shapes that are axisymmetric. The degree that this limitation would affect overall results should this assumption be violated has not been examined.

In addition, the small-perturbation theory method evaluated for this paper requires introduction of flow images to account for reflection of flow from an adjacent component. In these calculations, complete reflection has been assumed for the nacelle-on-wing interactions. In practice, for some geometric arrangements, partial reflections and refractions take place. Because of this, the theory is limited either to those configurations where the assumption of complete reflections is justified or where there are no reflections at all. The geometric arrangement that is most likely to be affected by this limitation is the situation of a nacelle partly ahead of the leading edge of a swept-wing. Such a case has been analyzed, however, and is reviewed in section 4.3.

3.4 Prediction of Nacelle-Installed Drag

Nacelle-installed drag calculated by the modified linear theory described above uses the superposition approach illustrated in figure 6.

Typically, the nacelle-installed drag is calculated as the sum of the friction drag of the nacelles, the net wave drag, and the lift interference effects.

The net nacelle wave drag includes--

- Nacelle pressure drag
- Nacelle pressures acting on the wing-body volume or thickness
- The wing-body thickness pressures acting on the nacelles
- Mutual nacelle interference

The mutual nacelle interference consists of the effect of the pressure field of a nacelle acting directly on the other nacelles plus the effect of the pressure field reflecting off the wing surface back onto the nacelles.

The lift interference consists of three items:

- The nacelle pressures reflecting off the wing produce an interference lift, ΔC_L. Because of the interference lift, the wing-body incidence required to produce a specified total lift is reduced, which results in a reduction in the wing-body drag-due-to-lift.
- The nacelle pressures acting on the mean lifting surface produce a drag or thrust force.
- The wing lifting pressures produce a buoyancy force on the nacelles.

The accuracy of current analytical methods of evaluating supersonic airplane drag depends on a detailed knowledge of the effective airplane shape. These theoretical methods, at present, represent the flow into the engines and the engine exhaust jets analytically as cylindrical streamtubes extending upstream of the inlet and downstream from the exhaust nozzle exit. However, since the pressure of the exhaust gases at the nozzle exit is generally different from ambient pressure, the jet will tend either to expand or to contract after leaving the nozzle. Additionally, for off-design conditions the engines may spill flow around the inlets. In principle, these deviations of inlet flow and/or jet exhaust from cylindrical streamtubes can result in aerodynamic interference on adjacent nacelle or airframe surfaces.

The effects of engine operating conditions on the surrounding flow field must therefore be considered in the drag calculations. An embedded flow analysis approach is discussed in this paper. In this approach, streamtube shapes are calculated for an isolated nacelle, depending upon the inlet and exit flow conditions. These streamtube shapes are treated as solid pseudo-nacelle shapes in subsequent fully supersonic flow analyses using the modified linear theory. The pseudo-nacelle shapes create pressure fields that can act on adjacent components. The pseudo-nacelles shapes cannot sustain buoyancy forces from these adjacent components. This requires a careful bookkeeping system.

4.0 TEST VERSUS THEORY COMPARISONS

This section contains a number of test versus theory comparisons to illustrate the validity of the theories that were discussed in the previous section. Results are typical of the more extensive comparisons presented in references 10 and 11.

4.1 Application of Theory to Simple Cases

Predicted aerodynamic characteristics of the NASA wind-tunnel model isolated wing-body configuration are compared with the corresponding test data in figures 7 and 8.

Drag predictions at zero lift were obtained as the sum of the volume wave drag calculated by far-field (area-rule) theory plus fully turbulent flow skin-friction drag. These drag predictions agree well with the test data.

The theoretical lift curve slopes also agree reasonably well with the test data. However, theory predicted the aerodynamic center too far aft, particularly at the low supersonic Mach numbers.

The good agreement between theoretical and experimental drag polars in figure 8 indicates that theory should predict the reductions in wing-body drag-due-to-lift associated with the nacelle interference lift (described in section 3.4).

Theoretical predictions of surface pressure distributions and zero-lift drag of the isolated nacelle at a mass-flow ratio of unity (i.e., no spillage) are compared with test data in figure 9.

Theoretical drag predictions agree with the test data at Mach 1.3 and 1.4. Theory overestimates the nacelle drag at Mach 1.2 and below. The Mach 1.15 pressure distribution shows that theory overestimates the expansion (i.e., negative) pressures on the nacelle boattail. This leads to the overestimation of drag at the lower supersonic Mach numbers. The pressure measurement at the first station at both Mach numbers is less than theory. This is probably due to the nacelle actually spilling a small amount of flow at the "mass-flow ratio unity" test condition.

4.2 Application of Theory to Nacelle Inlet Flow Fields

The effect of nacelle spillage (mass-flow ratios as low as 0.7) was investigated in the NASA nacelle-airframe interference test program. The mass flow through each nacelle was varied by a control plug in the flow-through sting supporting the nacelle. At supersonic speeds, a normal shock forms in front of the nacelle and moves progressively upstream as the mass fow through the nacelle is reduced.

Mixed subsonic-supersonic flow analyses were made of the isolated nacelle. The program used a time marching procedure to solve the unsteady two-dimensional "eddy viscosity" Navier-Stokes equations for turbulent flow of a nonconducting fluid. The method is described in reference 8. Viscosity effects were neglected in the analyses. With viscosity being neglected, the mixed-flow analysis program solves the Euler equations.

The calculations made were inviscid and axisymmetric and yield bow shock locations as part of the solution. A schematic of the flow field is shown in figure 10. Results of the computations include bow shock location and shape, flow field streamtubes, definition of subsonic flow regions, and nacelle surface static pressure distributions, as well as detailed flow field information (such as Mach numbers, pressures, velocitities) throughout the calculation region.

Calculations first were made for a 5-deg sharp-nose conical pitot inlet to validate the theory. The calculations were made for a freestream Mach number of 1.14 and for mass-flow ratios of 0.64, 0.81, 0.91. Mass-flow ratio equals the ratio of mass-flow rate of the spilling nacelle to the mass-flow rate without spillage.

Computed results are compared with experimental data from reference 12, in figure 11. The conical pitot inlet and the region near the inlet where the detailed flow field analyses were made are shown. Figure 11 also contains comparisons of predicted constant Mach contrours with experimental bow shock shapes that were determined from Schlieren pictures. The "bunched" upstream Mach contour lines, which were interpreted as predicted bow shocks, agree well with the test data. The calculations also indicate the presence of a significant region of subsonic flow between the inlet and the detached bow shock. The region of subsonic flow grows rapidly as the mass flow into the nacelle is reduced and more flow is forced to spill around the inlet. Figure 12 compares the predicted and experimental variation of shock standoff distance with mass-flow ratio.

Nacelle surface pressure measurements are compared with the corresponding theoretical predictions in figure 13. Reducing the mass-flow ratio is seen to have significant effect in decreasing the nacelle pressures near the inlet lip. Theoretical predictions agree quite well with test results.

The mixed flow analysis program was then used to calculate the inlet flow field about the NASA-Ames nacelle. Figure 14 shows the calculation mesh and analysis region.

Mach contours and streamtube shapes for flow into and around the nacelle were calculated for different mass-flow ratios and Mach numbers. Figure 15 shows typical results of these calculations.

Figure 16 summarizes the effect of reduced mass flow on the inlet flow field. The subsonic flow region between the detached bow shock and the inlet lip grows dramatically as the Mach number is reduced from 1.4 to 1.15. This figure also shows the location of the nacelle below the wing chord plane corresponding to the NASA-Ames nacelle-airframe wind-tunnel model arrangement. The subsonic flow region is seen to intersect the wing surface at Mach 1.15.

Nacelle theoretical surface pressure distributions were calculated for the forecowl of the NASA nacelle for various amounts of spillage at Mach 1.4 and 1.15. Theoretical pressure distributions are compared with test data in figure 17. The predicted effect of reduced mass flow on the nacelle pressure distributions agrees well with the test data.

Isolated nacelle drag calculations were made for various amounts of spillage. In these drag calculations, it was assumed the effect of spillage on skin friction drag was negligible. The nacelle wave drag with spillage was then calculated by adding the change in forecowl drag due to spillage to the total nacelle wave drag with no spillage. The predicted effect of spillage on isolated nacelle drag, as shown in figure 18, closely matches the test data.

These results indicated that the mixed flow theory program can predict satisfactorily the flow field characteristics around a spilling nacelle.

Predictions of interference pressures near the nacelle were made using the embedded-subsonic-flow analysis approach summarized in figure 19.

In this approach, streamtubes, which were defined by the mixed-flow theory, were analyzed as solid pseudo-nacelle shapes using the supersonic theory. Pressures predicted by these supersonic theory analyses were compared with the corresponding mixed flow theory predictions to assess the accuracy of the approach.

The bow-shock shape calculated by the supersonic theory for the nacelle with no spillage agrees well with the mixed-flow theory predictions, as shown in figure 20. The supersonic theory bow shock, however, does "bulge" forward of the mixed flow shock in the region near the inlet lip.

Calculated interference pressures surrounding the nonspilling nacelle are shown in figure 21 for various radial distances from the nacelle. The pressure signatures are quite similar except in the immediate vicinity of the bow shock. The mixed flow theory pressure rise is more gradual than that predicted by the supersonic theory. The more gradual pressure rise is attributed to the relative coarseness of the calculation mesh. These results tend to imply that the supersonic theory predictions of pressures surrounding a nacelle are accurate, provided the flow remains supersonic and the bow shock is of moderate strength.

Calculations were made of pseudo-nacelle geometries to evaluate procedures for using the supersonic theory to predict interference pressures for mass-flow ratios of 0.8 and 0.7. The pseudo-nacelle geometries included:

- Nacelle plus the capture streamtube
- Streamtube shapes surrounding the nacelle over which the flow remains supersonic; three streamtubes at various radial distances were analyzed

The calculated bow shock shapes for these various pseudo-nacelle shapes are compared with the mixed flow theory predictions for the spilling nacelles in figure 22.

The supersonic surrounding streamtubes corresponding to a specified mass-flow ratio all gave similar bow shock shapes and near-field pressure distributions. The capture streamtube results, however, differed from the supersonic surrounding streamtube results.

The shapes of the mixed flow theory bow shock and the supersonic surrounding streamtube bow shock are the same beyond radial distances of approximately two inlet diameters from the centerline. At smaller radial distances, the supersonic surrounding streamtube shock "bulges" forward of the mixed flow theory shock similiar to the no-spillage results shown in figure 20.

The bow shocks predicted, using the capture streamtube plus nacelle geometry, fall aft of the corresponding mixed flow theory shocks except very near the nacelle. Here, the supersonic theory shock waves incorrectly bulge forward of the start of the capture streamtube.

Figure 23 compares predicted interference pressure distributions for the spilling nacelles. The figure includes:

- Mixed flow theory results for spilling nacelles
- Supersonic theory predictions using capture streamline plus nacelle
- Supersonic theory predictions using supersonic surrounding streamtube

The mixed flow theory predictions were made using the actual nacelle shape and prescribed boundary conditions to provide the appropriate mass flow into the nacelle. The supersonic theory predictions were obtained from streamtube shapes defined by the mixed flow theory analyses. Inaccuracies in the prescribed streamtube shapes will therefore be reflected in the supersonic theory calculations. The no-spillage predictions of figure 2 implied that the mixed flow theory tended to "smear" the bow shock over two or three calculation-mesh cell widths. Hence, calculated streamtube shapes will also be overly smoothed. This would result in reduced shock strengths calculated using these shapes.

The previously mentioned differences in predicted bow shock strength are readily apparent in these comparisons. Moderate initial angle changes (approximately 2 deg) would account for the difference between the supersonic theory and the mixed flow theory bow shock strength predictions. Shapes of the pressure distributions computed using the supersonic surrounding streamtubes are similiar to the mixed flow theory results. Main features of the flow include a strong shock followed by a rapid expansion behind the shock, which is in turn terminated by a mild shock or flow recompression. Note that results obtained using the capture streamtube-nacelle representation do not give any indication of the strong expansion and mild recompression shock.

The results imply that normal-shock spillage interference can be properly calculated by using the following embedded subsonic flow approach.

1. Use the mixed flow theory to calculate the local flow field characteristics surrounding the spilling nacelle using a fine calculation mesh.
2. Compute the surrounding streamtube shapes.
3. Identify a near streamtube over which the flow remains supersonic.
4. Use this supersonic streamtube shape to calculate the pressure field surrounding the spilling nacelle.
5. Integration of the spilling nacelles pressure on the wing surface and an adjacent nacelles should provide the interference forces.

4.3 Application of Theory to Prediction of Nacelle Interference on Adjacent Airplane Components

Figure 24 contains a comparison of predicted and measured mutual nacelle interference drag for various nacelle stagger arrangements. The mutual nacelle interference is the result of the pressure field of each nacelle pushing on each of the other nacelles. The measured mutual nacelle interference was obtained as the difference in the drag of the nacelles with and without the other nacelles present. Theoretical predictions agree well with test data.

Theoretical nacelle shock-wave patterns and interference pressures on the wing lower surface are compared with test data for one of the aft unstaggered nacelle location in figures 25 and 26. The experimental interference pressures were obtained as the difference in the wing lower surface pressures with and without the nacelles present.

The predicted nacelle bow-shock locations agree well with the experimental shock locations, as indicated by a sudden "jump" in interference pressures, ΔC_p, from zero to a large positive value. Theoretical interference pressure distributions agree reasonably well with the experimental data. The experimental bow-shock strength is less than indicated by the test data. This may be the result of a shock boundary-layer interaction softening this initial sudden pressure rise.

Figure 27 contains a comparison of predicted shock-wave patterns and interference pressure fields with test data for a forward unstaggered nacelle location in which the outboard nacelle is near the wing leading edge. In this nacelle arrangement, the wing experiences not only the bow shocks from the nacelles, but also aft shocks. The aft shocks arise from the flow compression at the aft end of the nacelle where the flow-through sting enters the nacelle shell.

The predicted and measured interference pressures for this wing-body forward nacelle arrangement agree quite well except in local areas near the aft shock and at the most outboard station.

In reference 9 it is shown that flow across a glancing shock wave, in which the flow is deflected in the plane of the wing, will separate if the pressure rise across the shock wave exceeds 50%. Furthermore, it is shown that a local negative pressure field on the wing can amplify the pressure rise across a shock wave.

Theoretical bow shock and aft shock strengths on the wing lower surface are compared with this shock-induced boundary layer separation criteria (ref. 10) in figure 27. The aft shocks are seen to be sufficiently strong to cause boundary layer separation. Indeed, this separation is evident by the discrepancy between the theoretical predictions and test data in the areas near the aft shocks.

Figures 28 and 29 contain experimental and calculated shock wave patterns, and interference pressures on the wing lower surface for conditions in which the nacelles are operating at a mass-flow ratio of approximately 0.8. The theoretical shock-wave patterns for no spillage are also shown for reference. The theoretical predictions are in fair agreement with the test data.

The theoretical calculations for the spillage conditions were made using supersonic theory and pseudo-nacelle geometry consisting of the actual nacelle geometry plus the capture streamtube as inlet extensions. The more accurate supersonic surrounding streamtube method was not used because the previous mixed-flow analyses were restricted to the inlet region only. As a result, the full shapes of the surrounding streamtubes were not defined.

4.4 Installed Nacelle Lift and Drag

Comparisons between theoretical and experimental nacelle lift and drag are shown in figures 30 and 31 for an aft unstaggered nacelle location. The drag comparisons include the net interference on the wing-body, the net interference on the nacelles, and the total nacelle installation drag. The drag and lift predictions agree quite well with the test data.

This aft nacelle location is seen to be a favorable low-drag installation, since at moderate lift coefficients the installed nacelle drag is less than half the isolated nacelle drag level. This favorable effect is primarily due to the reduction in wing-body drag-due-to-lift associated with the nacelle interference lift.

The measured interference lift increment increases with angle of attack, particularly at Mach 1.15. The theoretical interference lift calculations were made at a constant local Mach number equal to the freestream Mach number. The increase in interference lift can be attributed to a reduction in the local Mach number around the nacelles associated with the change in the wing interference pressure fields as angle of attack is increased. This effect is the greatest at very low supersonic Mach numbers.

Similar test versus theory comparisons are shown in figure 32 for a forward nacelle location at Mach 1.4. The theoretical predictions differ significantly from the test data. This difference is believed to be due to two effects: (1) shock-induced separation associated with the strong nacelle aft shocks, and (2) influence of the nacelle pressure field affecting the upper surface of the wing. Neither of these effects is included in the theory. However, both theory and test indicate that the nacelle interference effects for this forward location are highly unfavorable. The installed drag increases with angle of attack and approximately doubles the isolated nacelle drag level.

Figures 30, 31, and 32 show that nacelle location can have a powerful effect on the nacelle interference. At the aft nacelle locations, both the interference of the nacelles on the wing-body and the wing-body on the nacelles are favorable. The nacelles in the aft locations produce a substantial level of favorable interference. As the nacelles are moved forward, both of these interference components become unfavorable, which results in considerable unfavorable net interference.

Figure 33 contains comparisons of calculated nacelle interference drag with test data for different mass-flow ratios; i.e., amounts of spillage. The drag of the isolated nacelle, measured at the average mass flow for the nacelles at each nominal test condition, was removed from the corresponding measured total wing-body nacelle drag. Similarly, the theoretical interference drag predictions do not include the calculated isolated nacelle drag.

The effect of spillage on the nacelle interference acting on the wing-body appears to be correctly predicted by the theory.

The effect of spillage on the interference on the nacelles is less than predicted by theory. Consequently, the theoretical effect of spillage on the total nacelle-installed aerodynamic interference drag does not agree very well with the test data.

4.5 Application of Theory to Jet Exhaust Interference

The shape of exhaust plume of a jet engine can provide an additional source of aerodynamic interference. One approach to predict these interference effects is to represent the jet plume by an equivalent solid body extension. Calculations of aerodynamic interference with and without the solid body extensions would provide an assessment of the jet exhaust interference on the adjacent components of the airplane.

NASA conducted an experimental investigation to verify the concept of representing a jet equivalent solid body. The exhaust-nozzle simulation system used in the study is shown in figure 34. Full details of the study are reported in reference 13.

Experimental data from this NASA test program were used to assess the accuracy of the supersonic theory (described in section 3.2) for predicting jet exhaust interference. Theoretical predictions were made of the pressures surrounding the nozzle simulator with the jet shape determined by inviscid theory. Theoretical predictions are compared with test data in figure 34.

Predictions obtained using the inviscid jet shape agree closely with measurements around the actual exhaust jet. These results indicate that the concept of representing a jet plane by a corresponding equivalent solid body shape is valid, and that supersonic theory can predict these effects.

5.0 CONCLUDING REMARKS

Because an extensive experimental data base was made available by NASA, it has been found possible to evaluate the validity of theory as applied to the difficult problem of airframe-propulsion system aerodynamic interference at high transonic Mach numbers including off-design engine mass-flow effects. It was found that practical theoretical methods are now available to address this problem quite satisfactorily. Success was achieved by selecting the simplest applicable theory, examining its inherent limitations, and correcting these limitations selectively and locally.

The configurations examined were limited to wing-body combinations with axisymmetric nacelles. Future work should emphasize departures from axisymmetry in nacelle geometry. To do this, it will first be necessary to carry out experiments, comparable in quality to those used in this paper, with other nacelles. It will then be necessary also to develop corrections to the theory to account for nacelle shapes that are significantly different from those for which the theories used in this paper were developed.

It was not found possible to evaluate the theories used in this paper in the Mach region from 0.95 to 1.05. As the regions of subsonic flow embedded in the main supersonic stream increase in size, procedures that have been shown to work fairly well at Mach 1.05 will eventually fail as Mach number is reduced from that value. Eventually, at Mach numbers less than 0.95, what has been used in this paper should work in principle, but different elemental computer programs will have to be used. The problem now becomes one of supersonic flow pockets in a main subsonic field.

All in all, however, the work presented here has shown that theory can help to understand interference effects of spilling nacelles; and that calculations, using these theories, should help airplane designers avoid nacelle installations that would have high inherent interference drag.

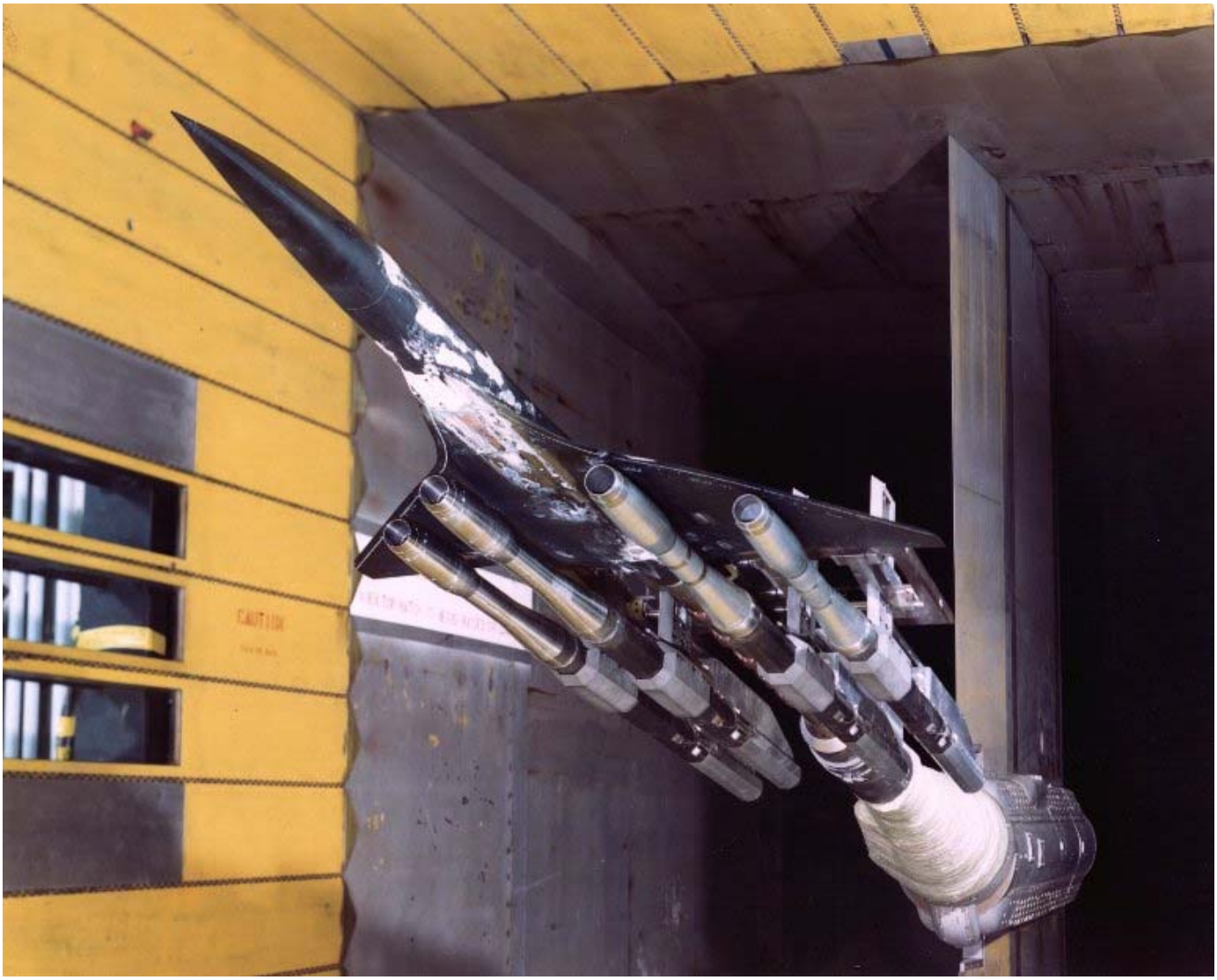

Figure 1 NASA Nacelle – Airframe Interference Wind Tunnel Model

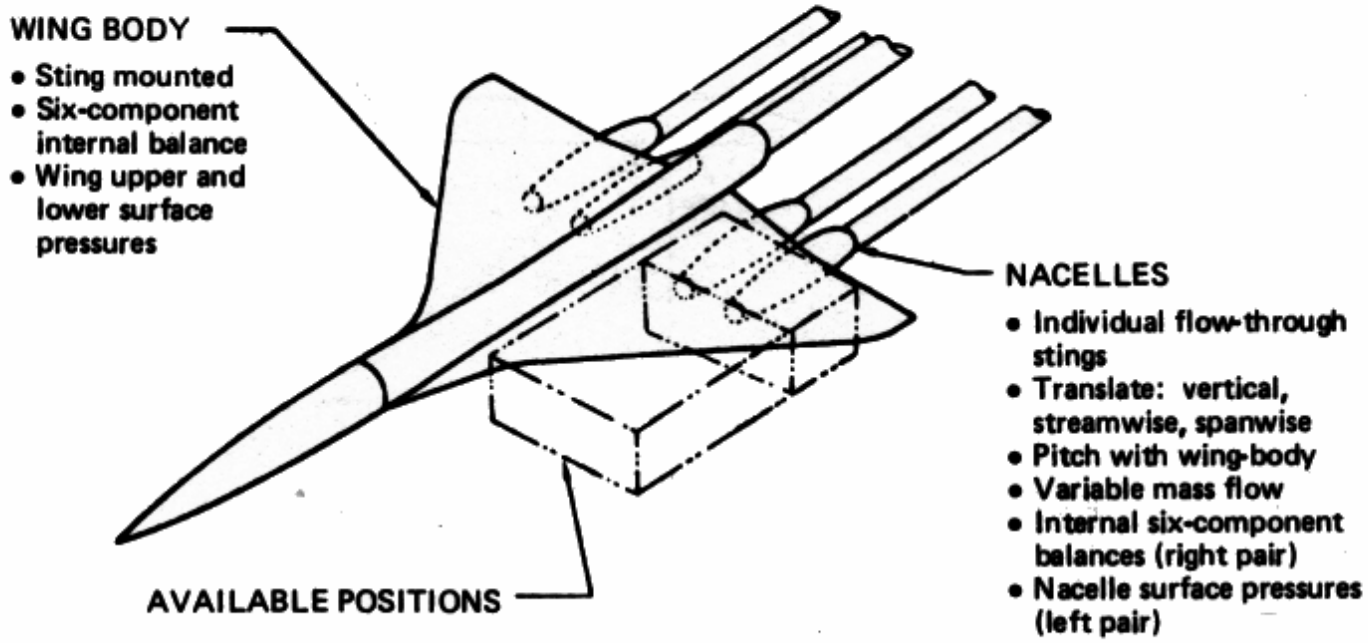

Figure 2. Wind Tunnel Model Features

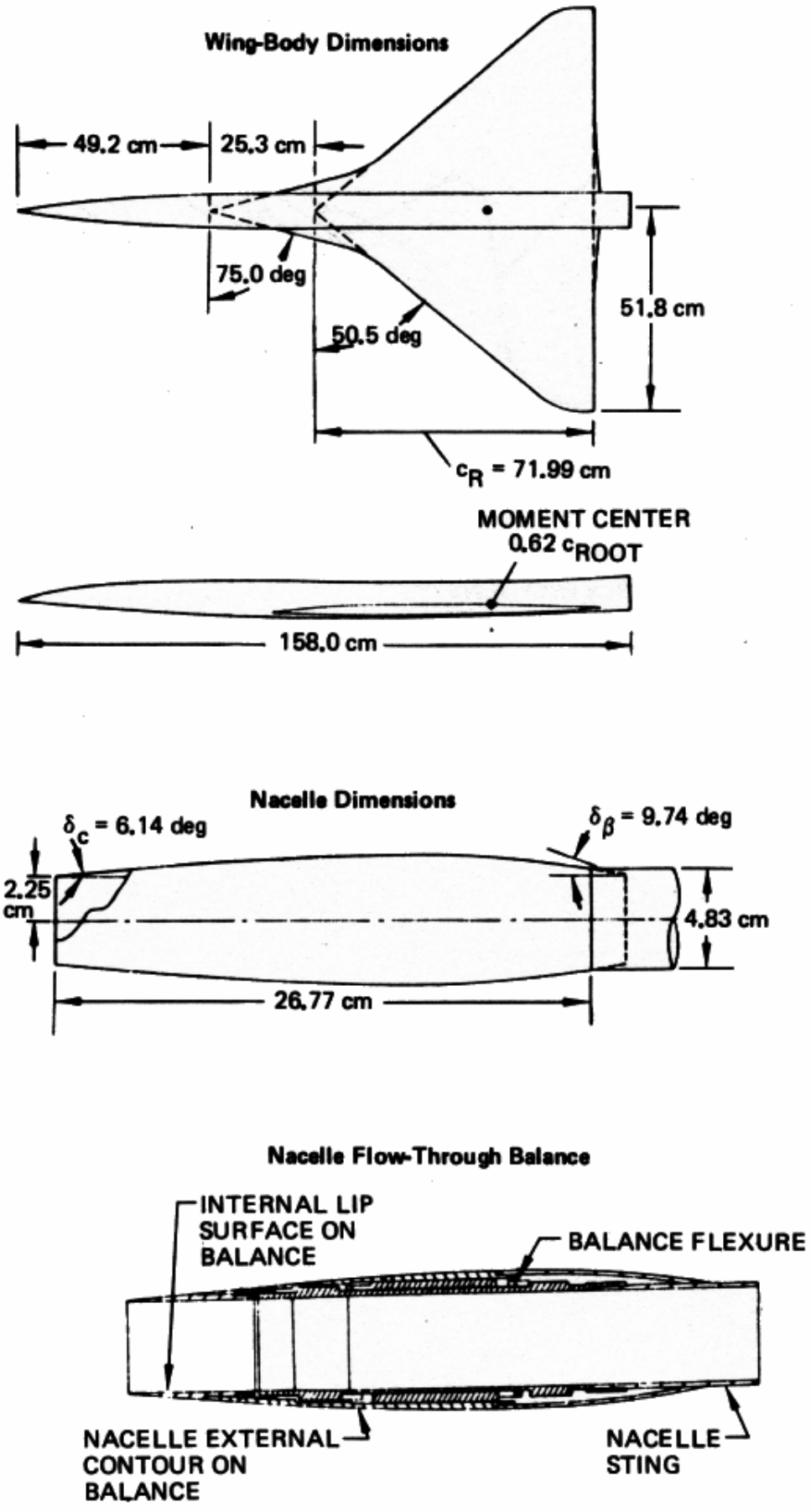

Figure 3. Wind Tunnel Model Dimensions and Details

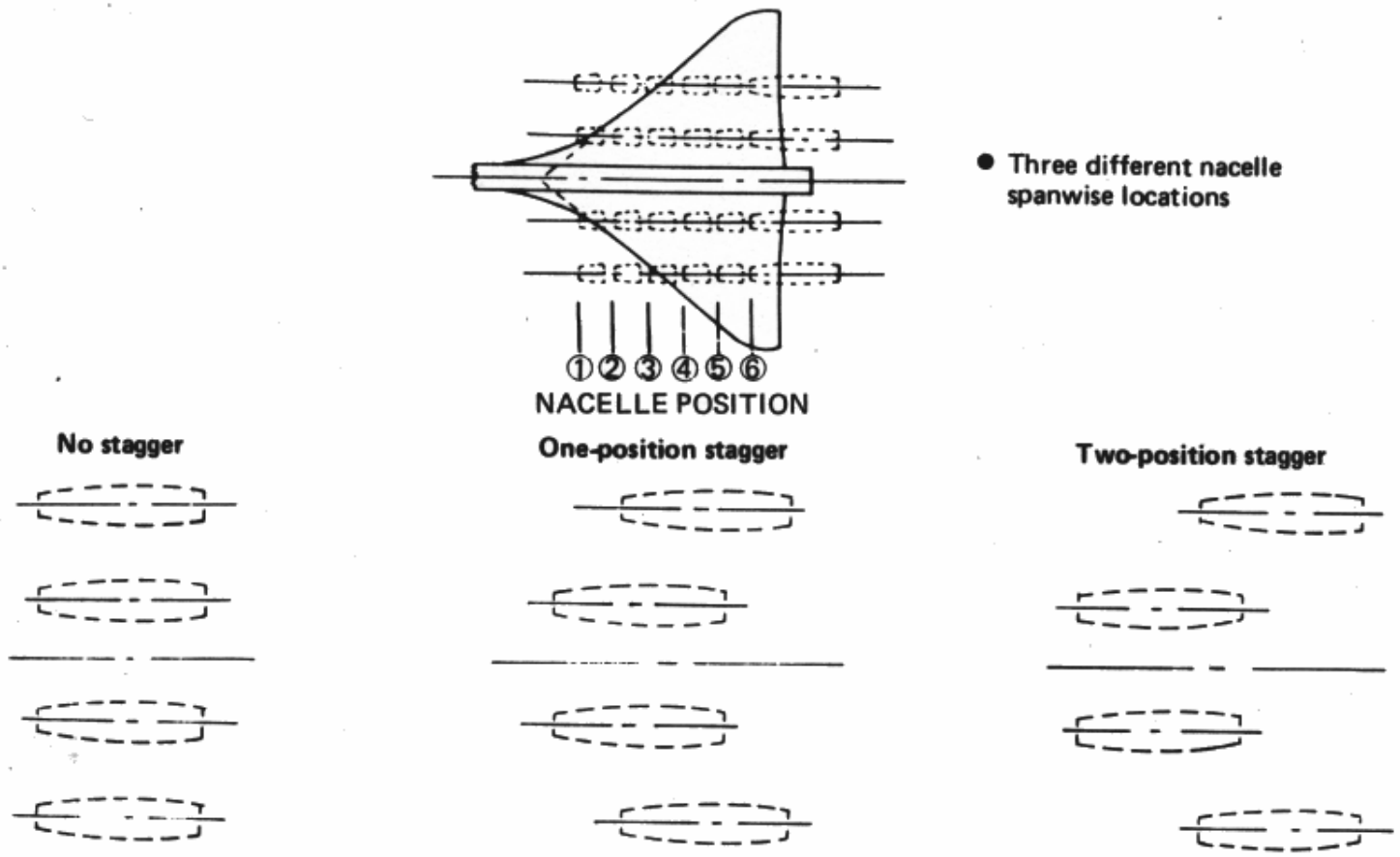

Figure 4. Tested Nacelle Locations

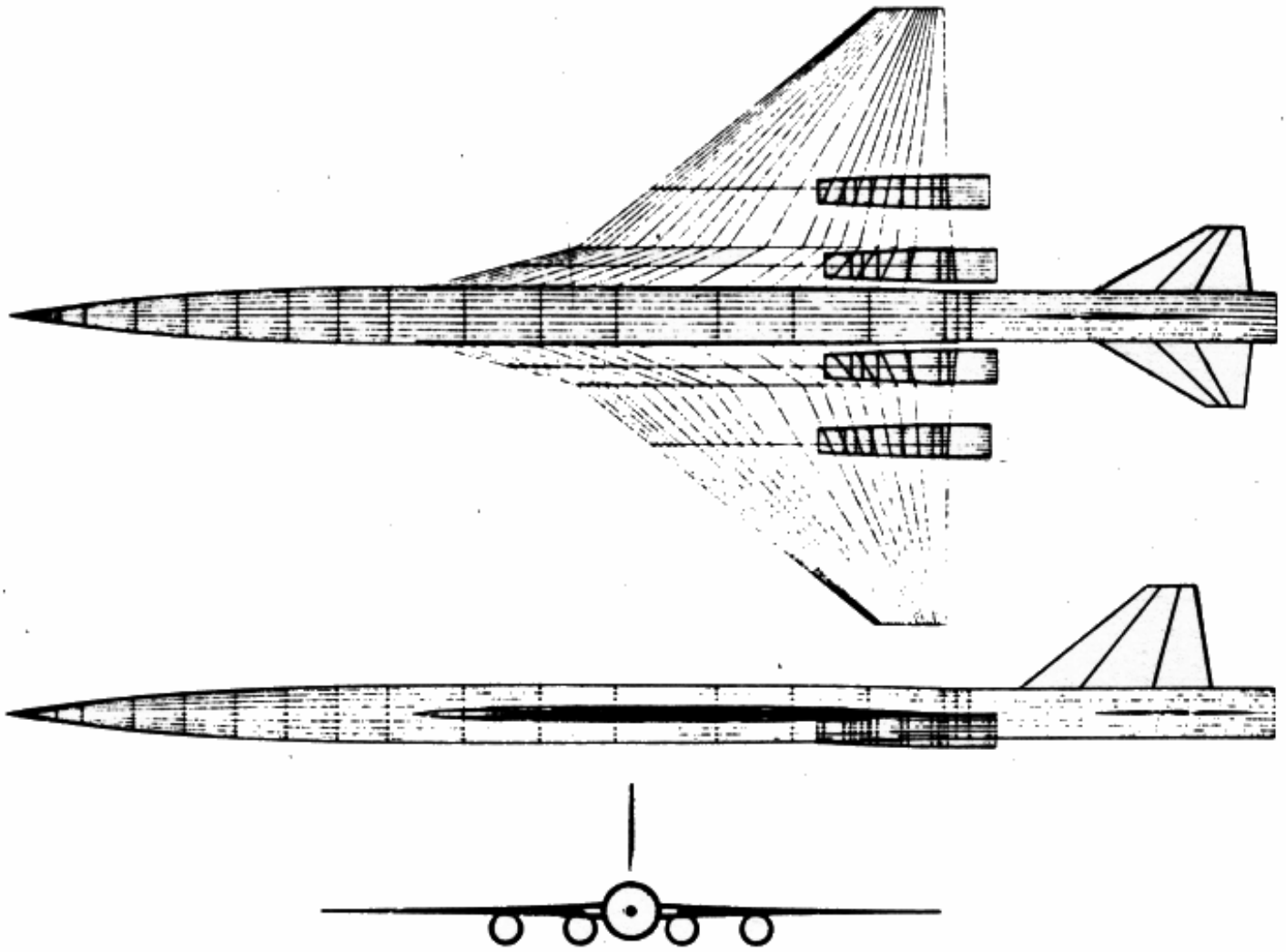

Figure 5. Linearized Supersonic Transport Wind-Tunnel Model Geometry

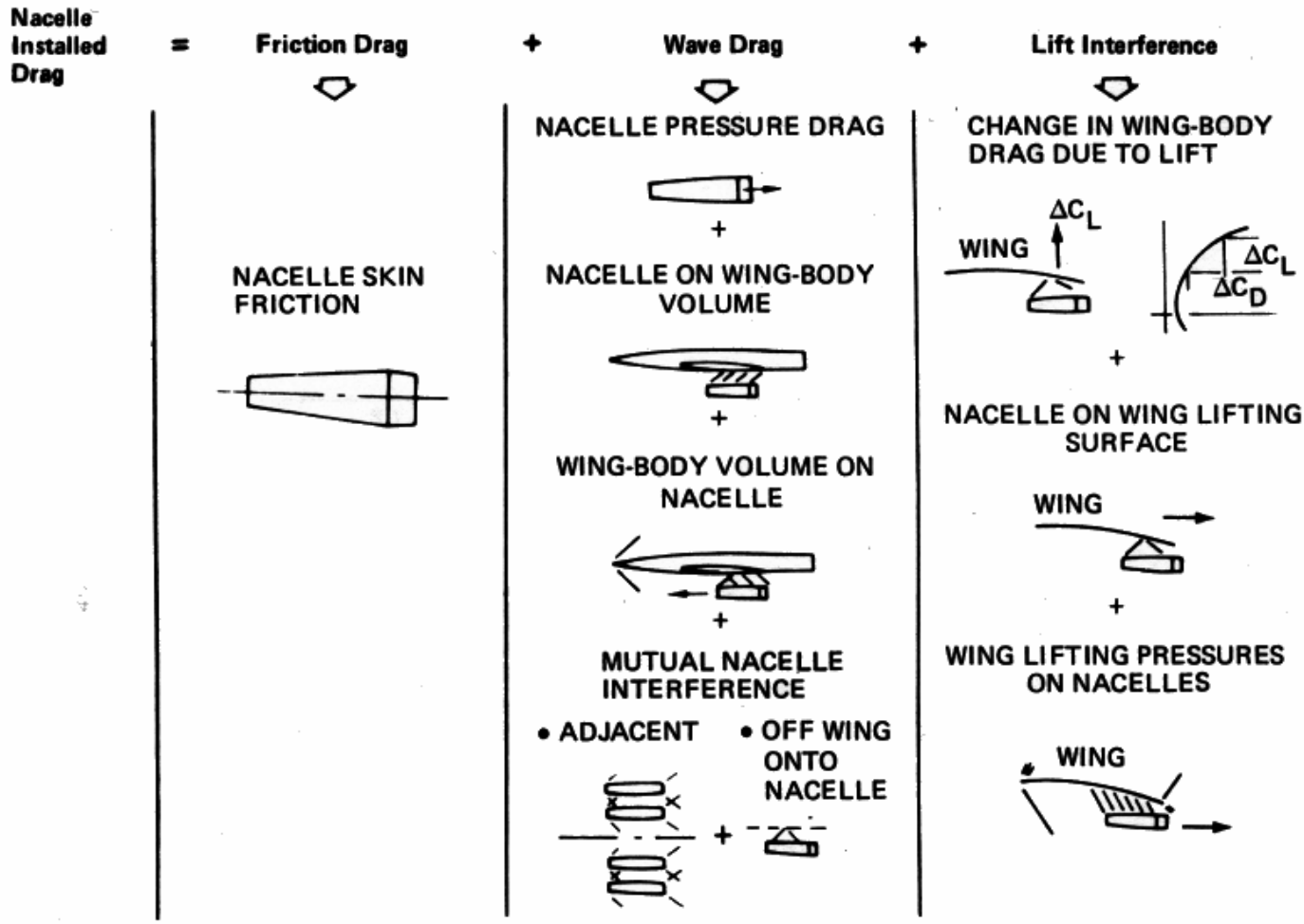

Figure 6. Nacelle Installed Elemental Drag Components

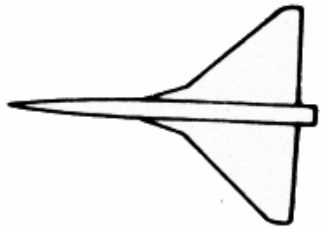

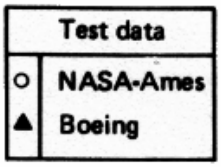

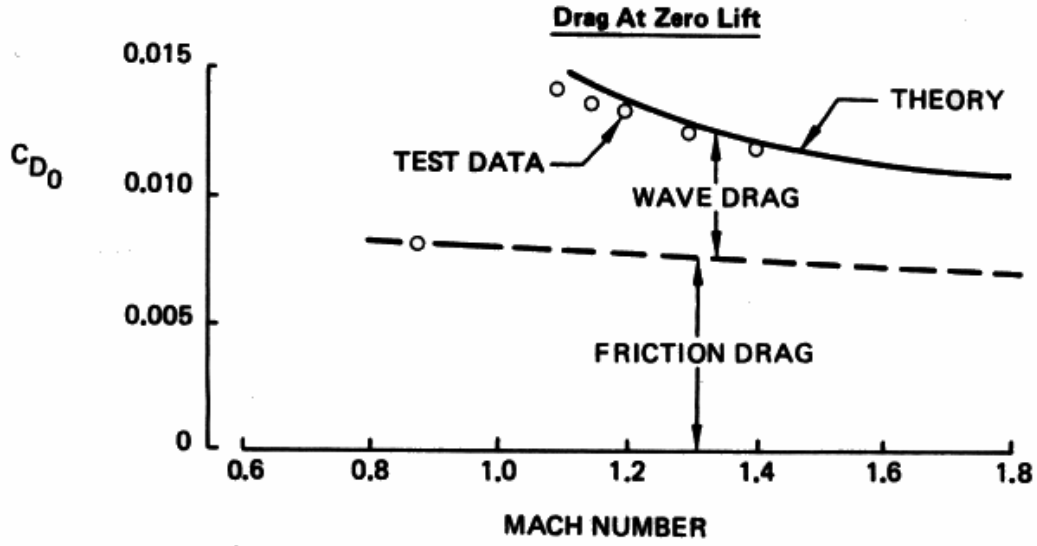

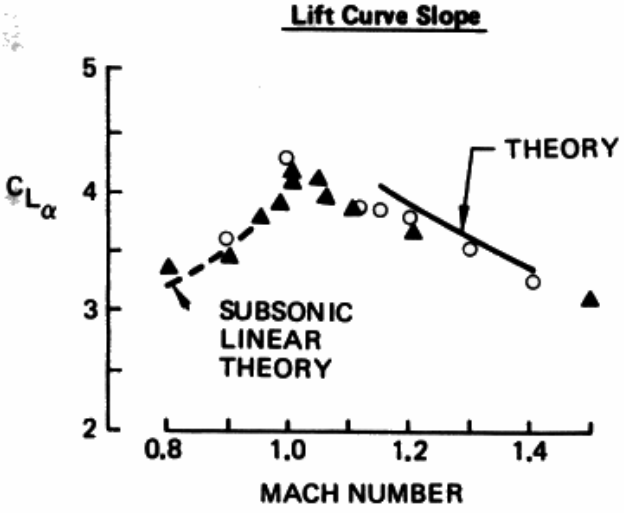

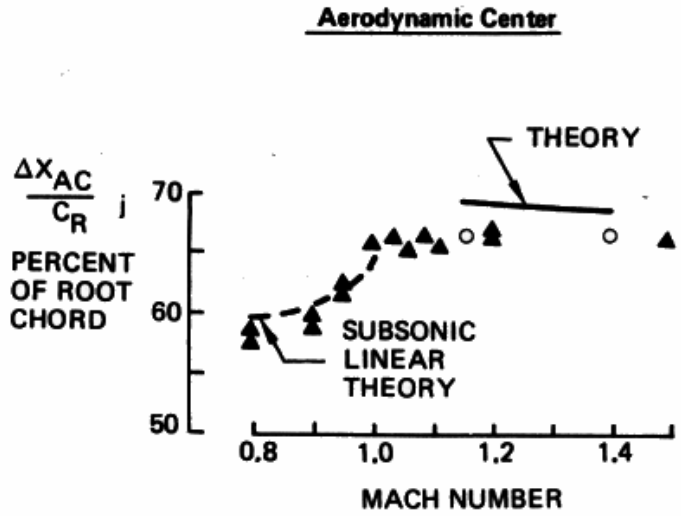

Figure 7. Wing-Body Lift, Drag, and Pitching Moment Comparisons at Zero Lift

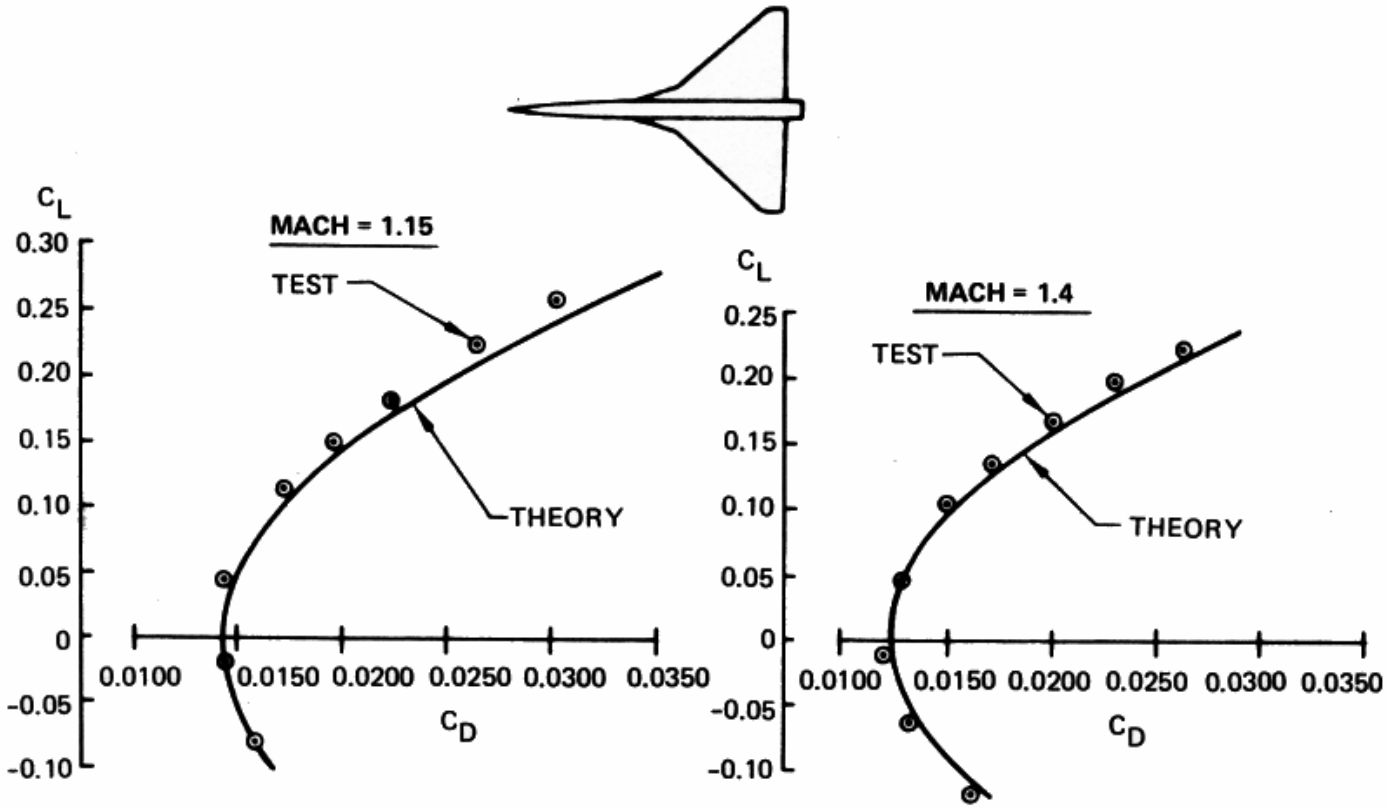

Figure 8. Variation of Wing-Body Drag With Lift

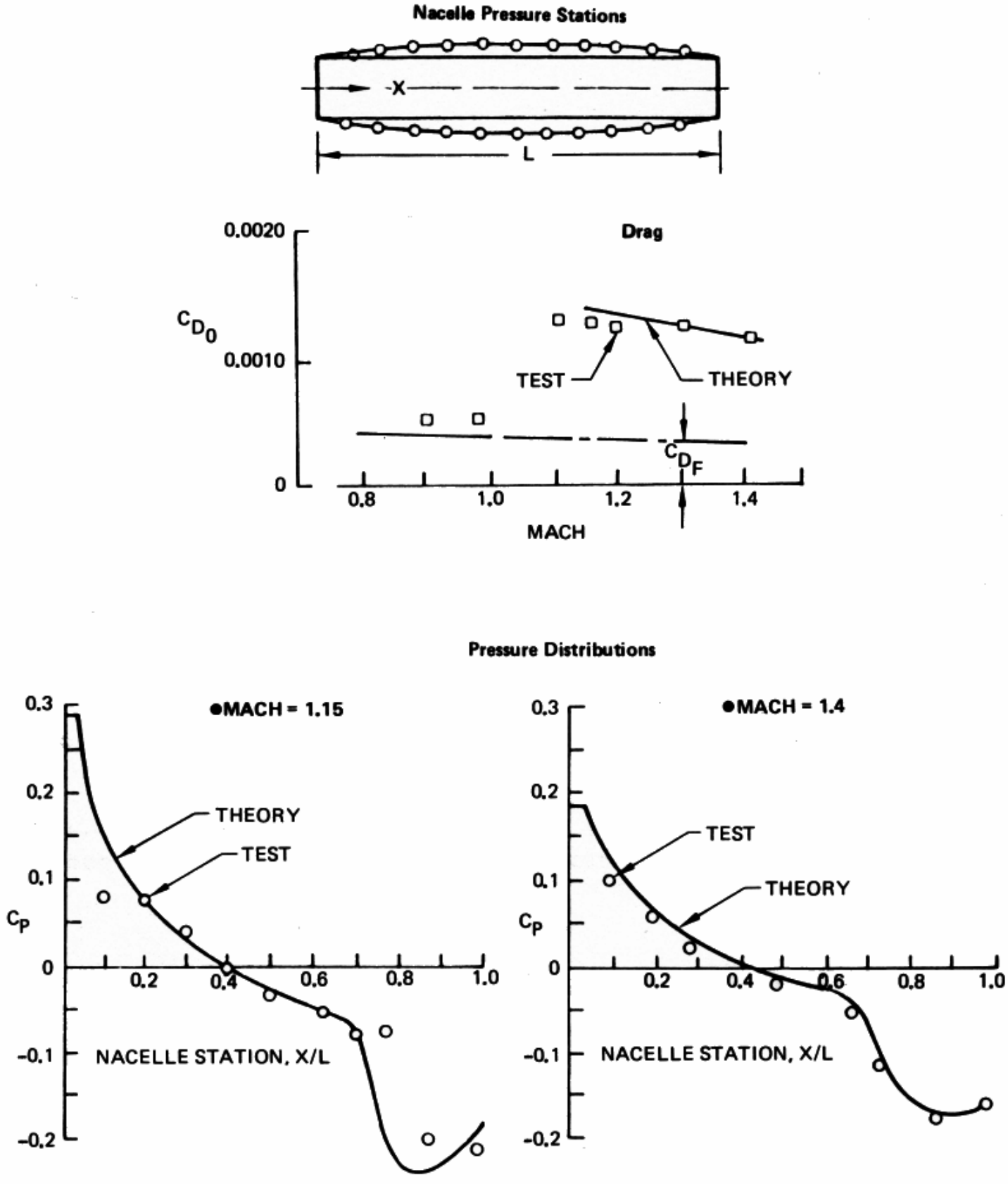

Figure 9. Isolated Nacelle Pressure Distributions and Drag at Zero Angle of Attack and a Mass Flow Ratio of Unity

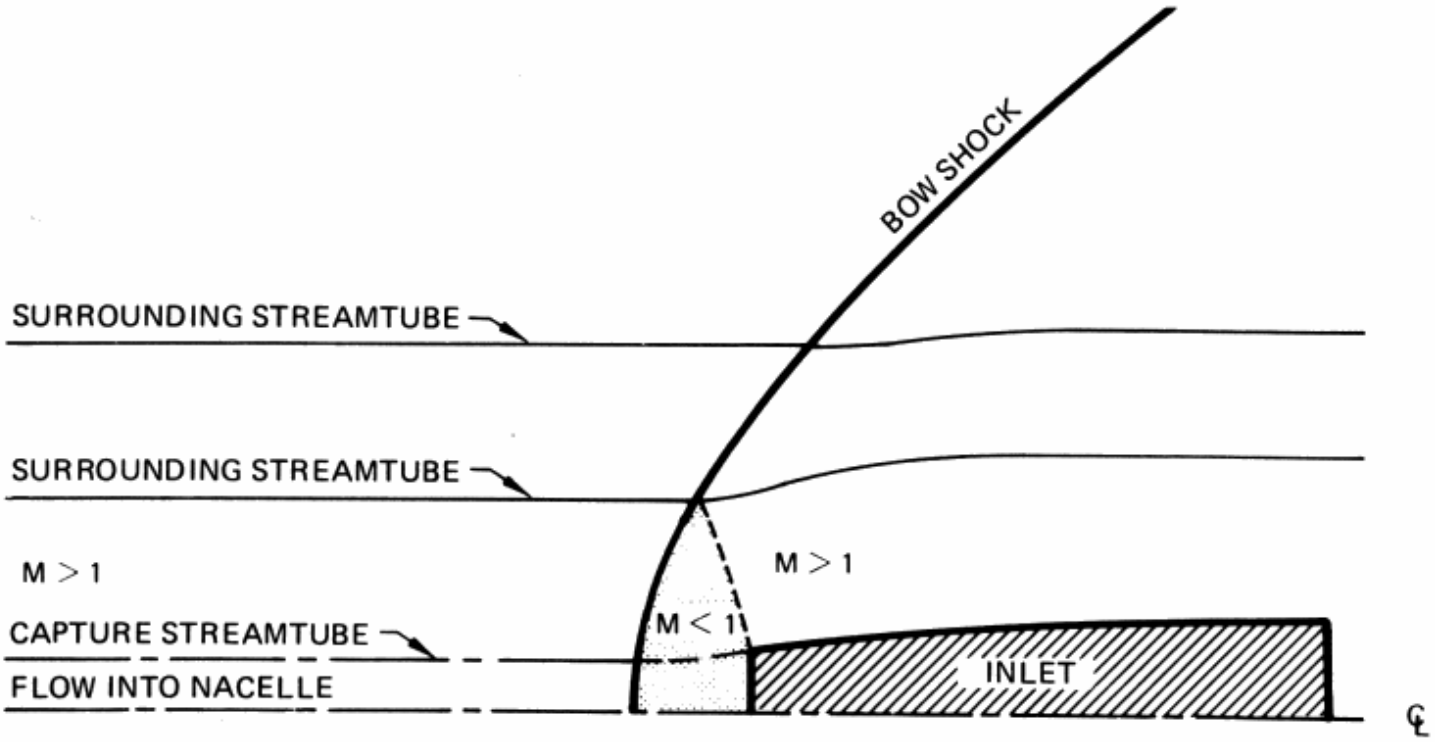

Figure 10. Schematic Diagram of Supersonic Pitot Inlet Flow Field for Mass-Flow Ratio Less Than Unity

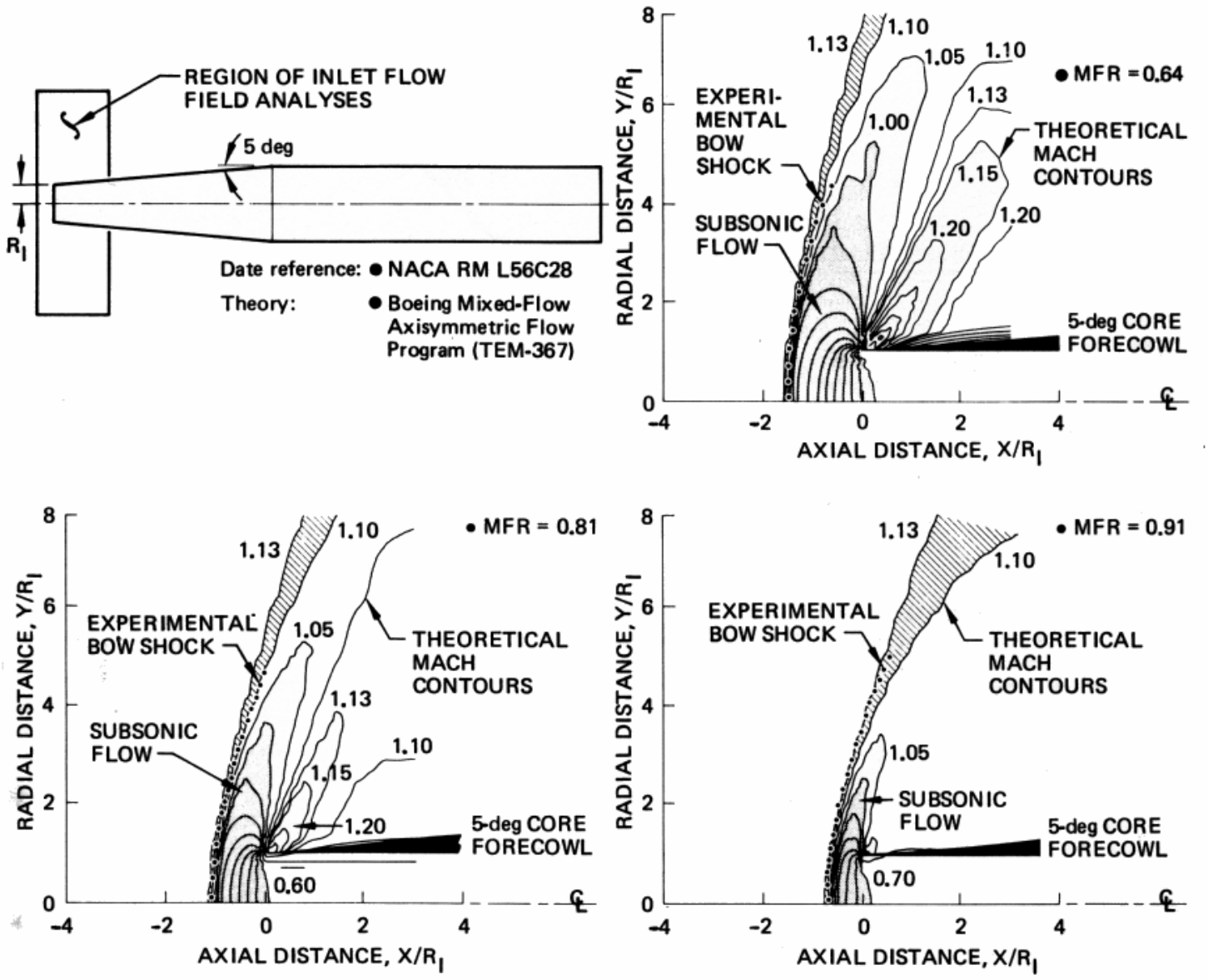

Figure 11. Verification of the Mixed-Flow Theory

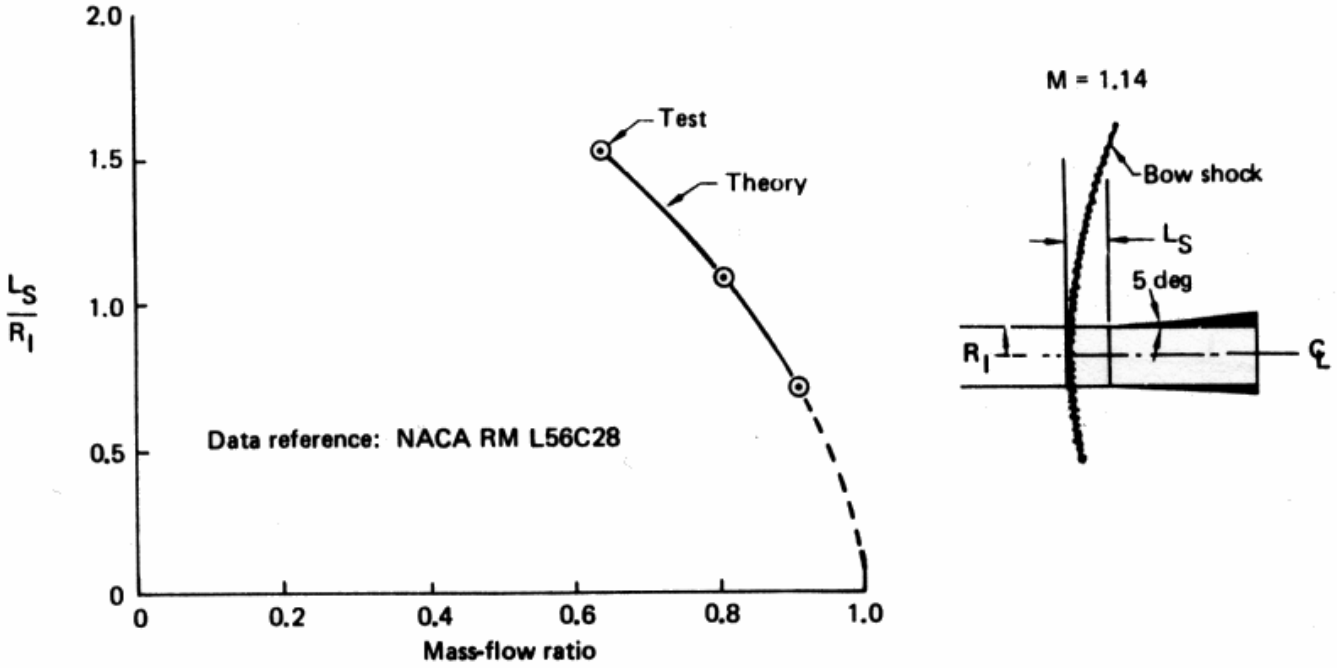

Figure 12. Effect of Mass-Flow Ratio on Shock Standoff Distance

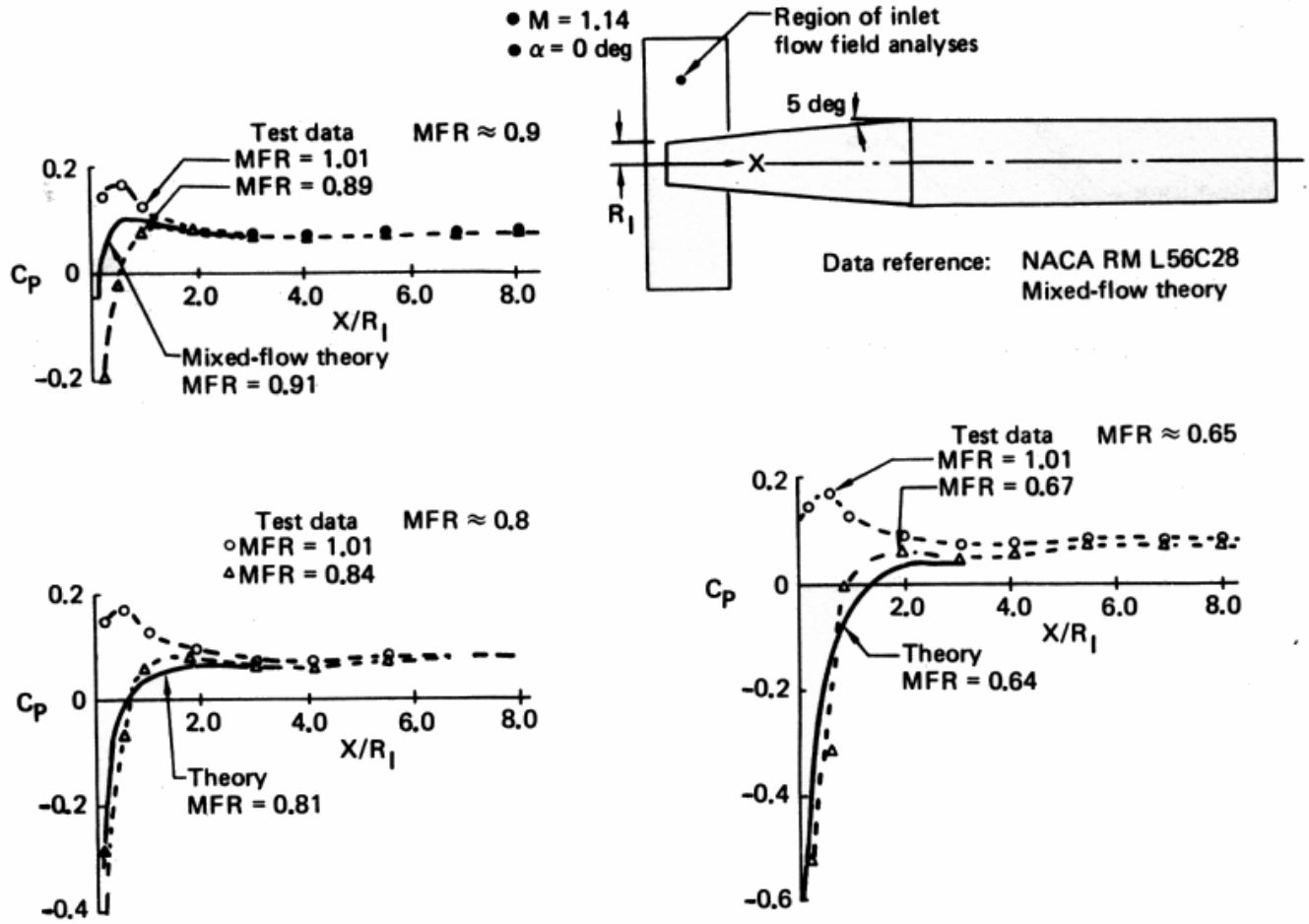

Figure 13. Effect of Mass-Flow Ratio on Conical Inlet Surface Pressures

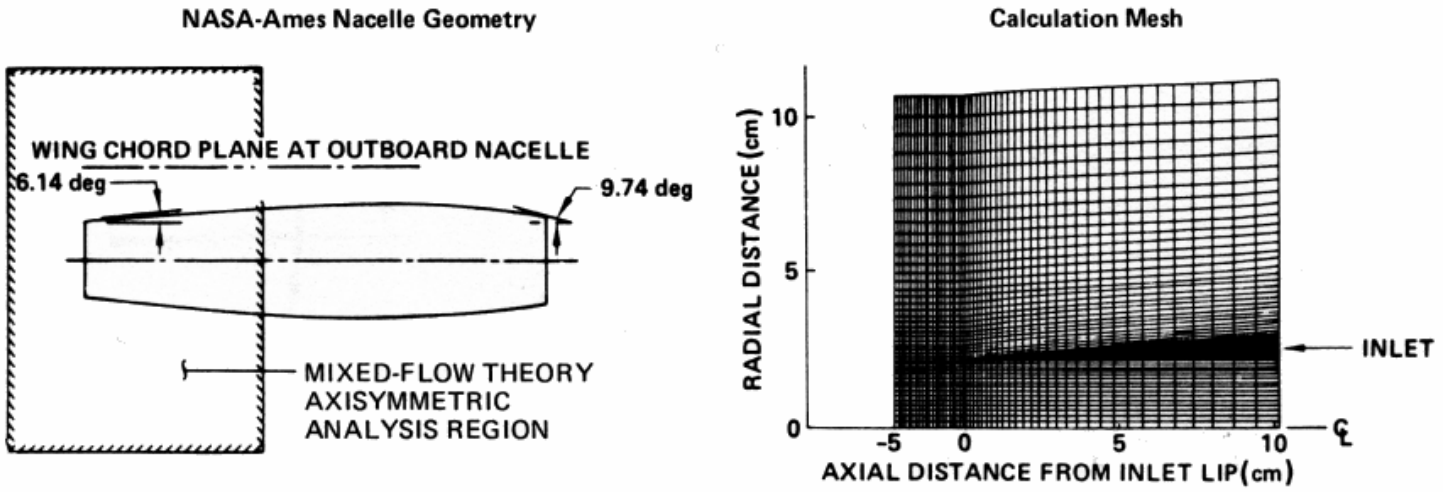

Figure 14. Mixed-Flow Analysis Geometry

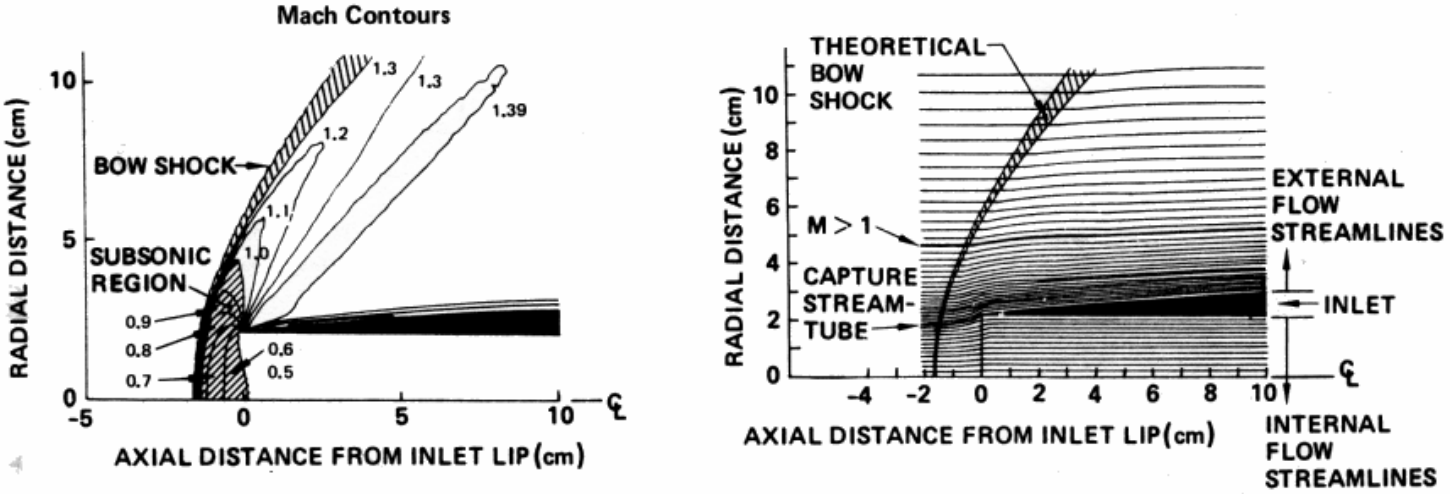

Figure 15. Mixed-Flow Analysis Results at Mach 1.4 and a Mass Flow Ratio of 0.7

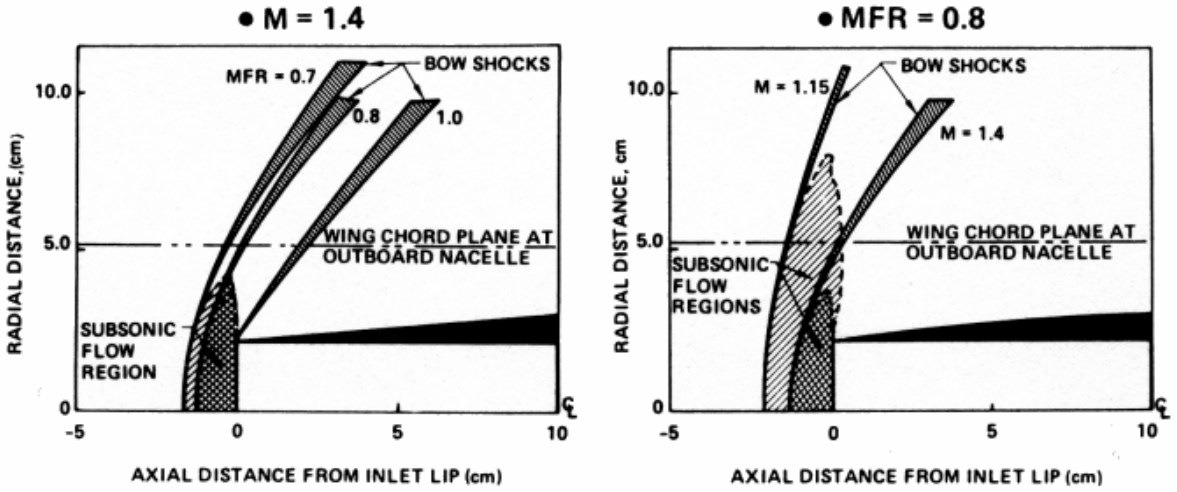

Figure 16. Effect of Spillage on Inlet Flow Field

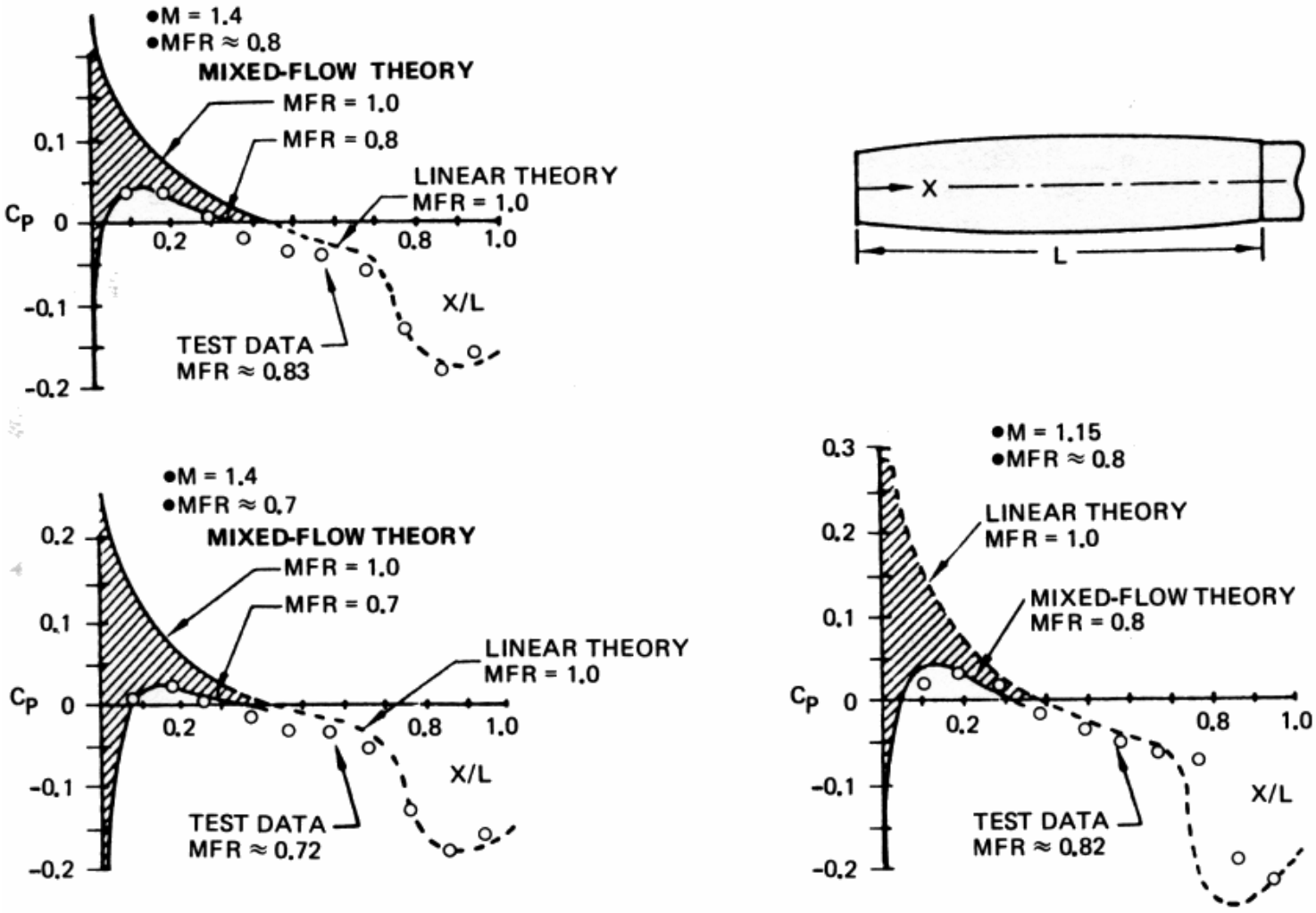

Figure 17. Effect of Spillage on Nacelle Isolated Pressures

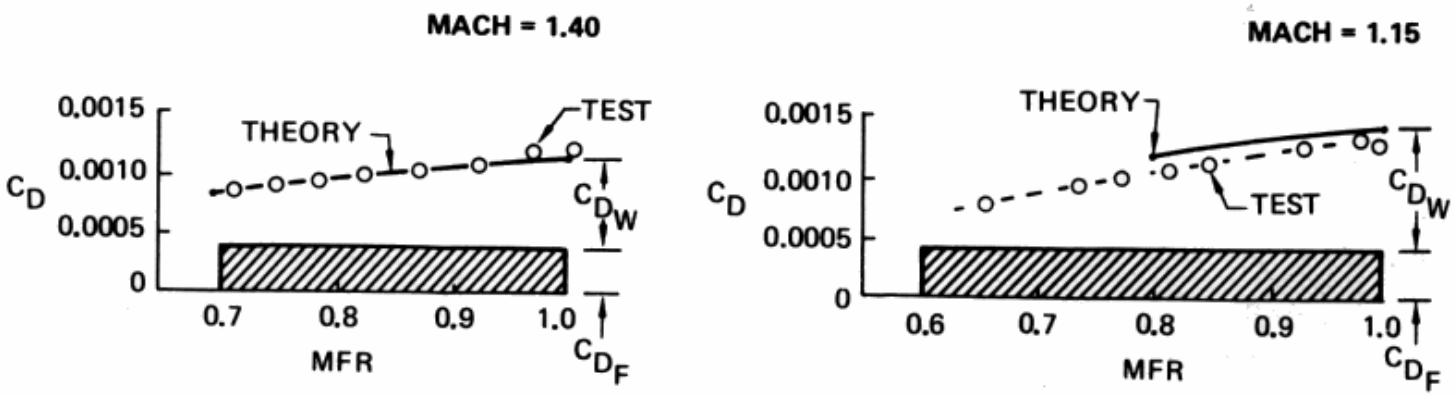

Figure 18. Effect of Spillage on Isolated Nacelle Drag

STEP 1: MIXED-FLOW ANALYSES OF FLOW FIELD SURROUNDING INLET

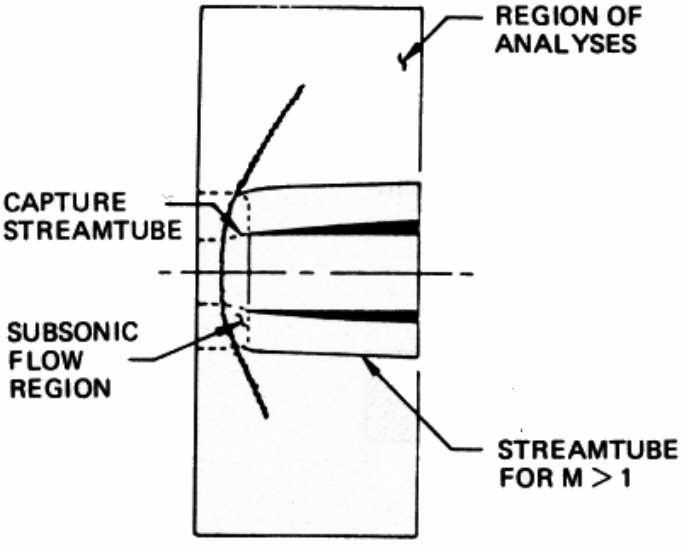

STEP 2: COMPUTE SURROUNDING STREAM-TUBE SHAPES

- INLET WITH CAPTURE STREAMTUBE

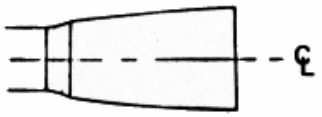

- M > 1 STREAMTUBE

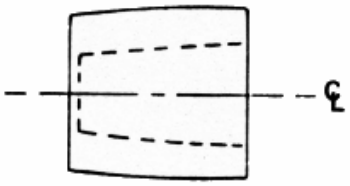

STEP 3: USE SUPERSONIC THEORY TO PREDICT INTERFERENCE PRESSURES FOR PSEUDO-NACELLE SHAPES CORRES-PONDING TO SURROUNDING STREAMTUBES

STEP 4: COMPARE WITH MIXED-FLOW ANALYSES PRESSURE PREDICTIONS

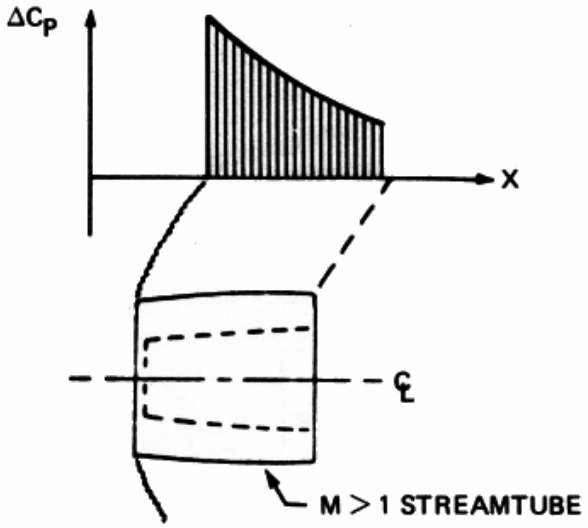

Figure 19. Embedded-Subsonic-Flow Interference Analysis Approach

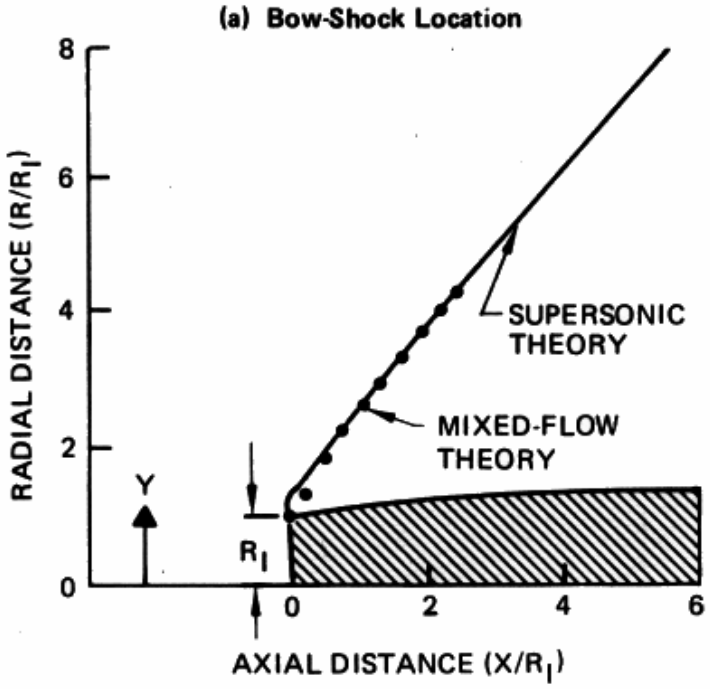

Figure 20. Comparison of Predicted Bow-Shock Characteristics at Mach 1.4 With a Mass-Flow Ratio of Unity

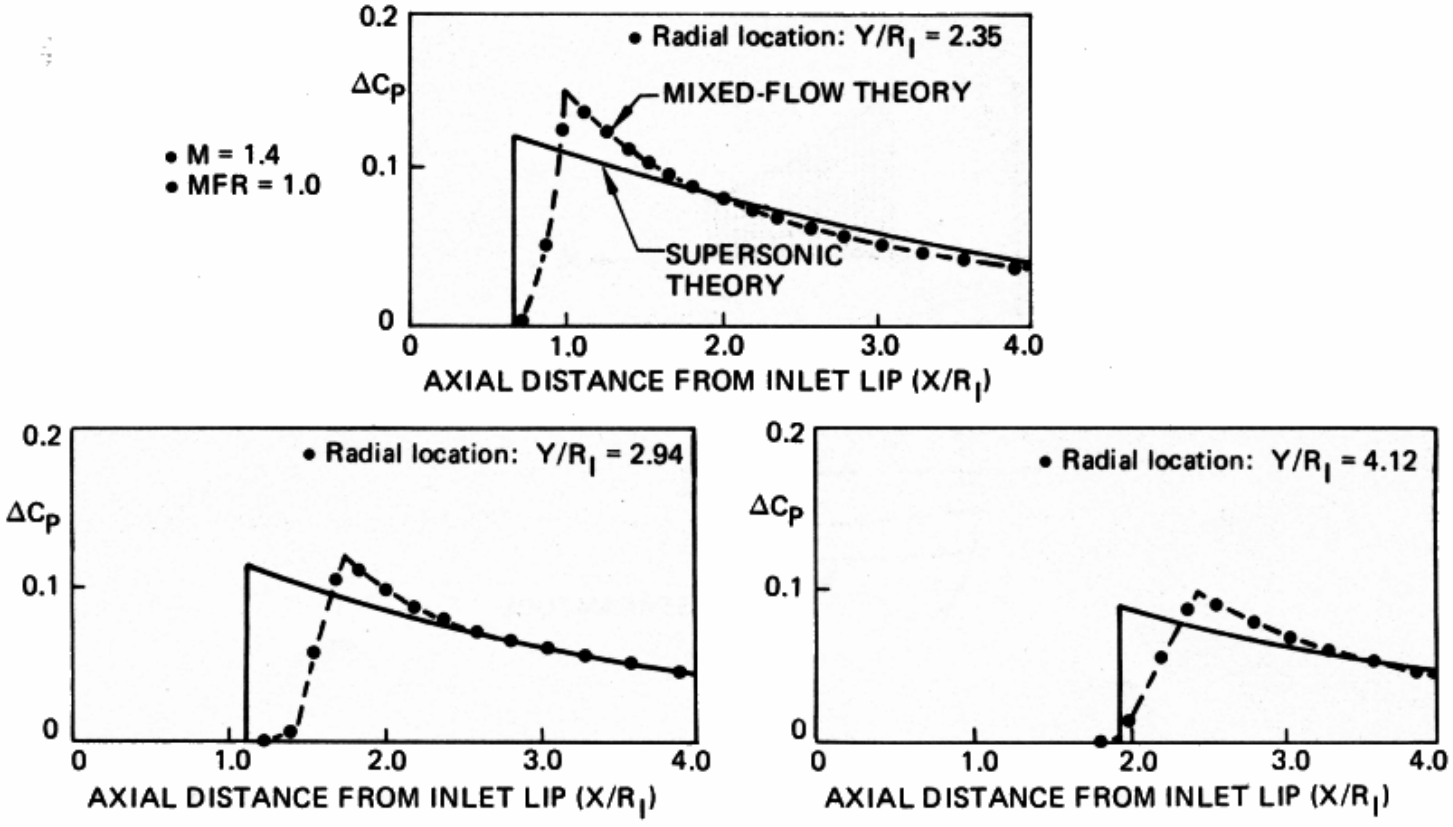

Figure 21. Comparison of Interference Pressures Near a Nonspilling Nacelle at Mach 1.4

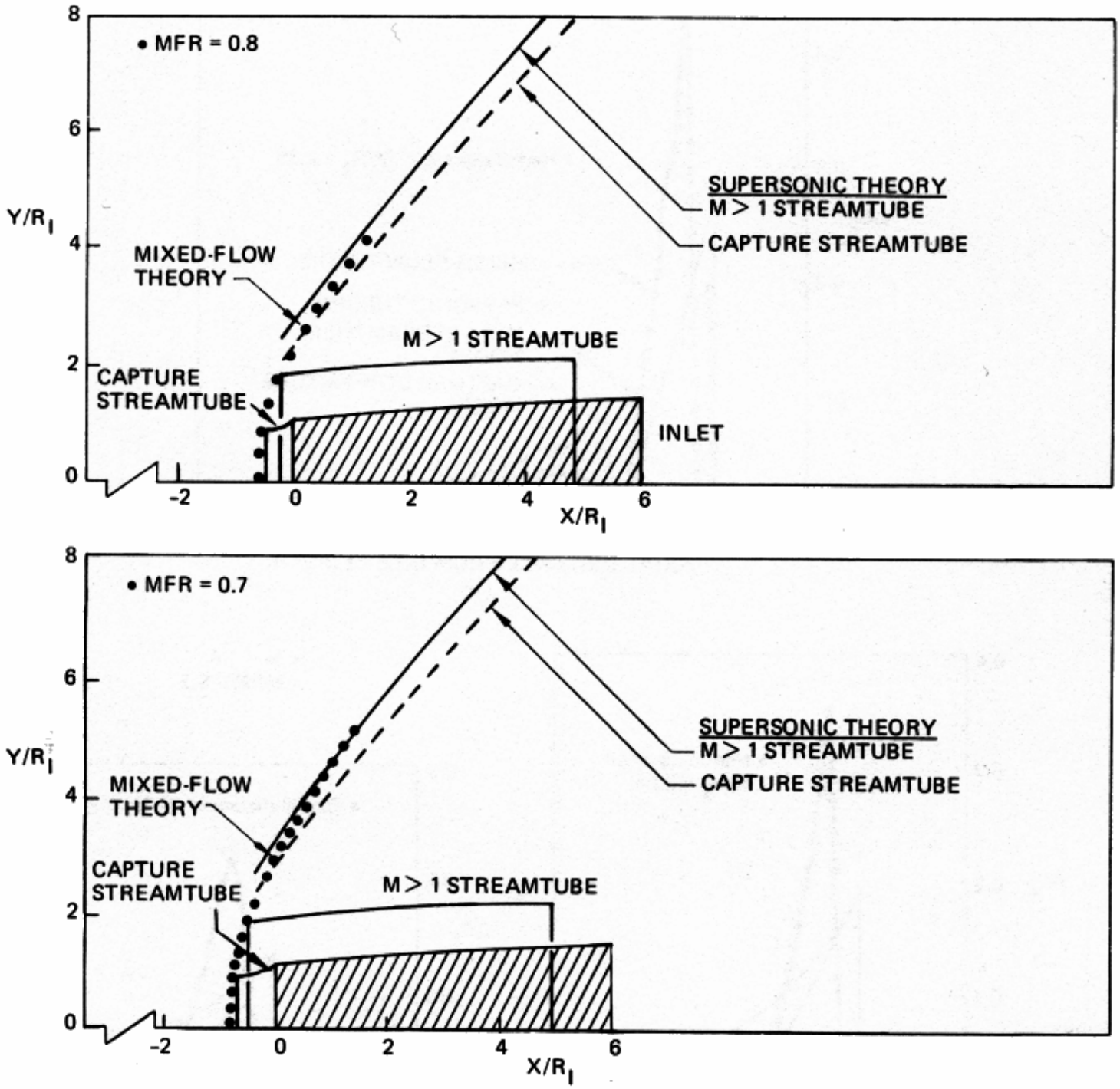

Figure 22. Comparison of Predicted Bow-Shock Shapes for Mass-Flow Ratios of 0.7 and 0.8 at Mach 1.4

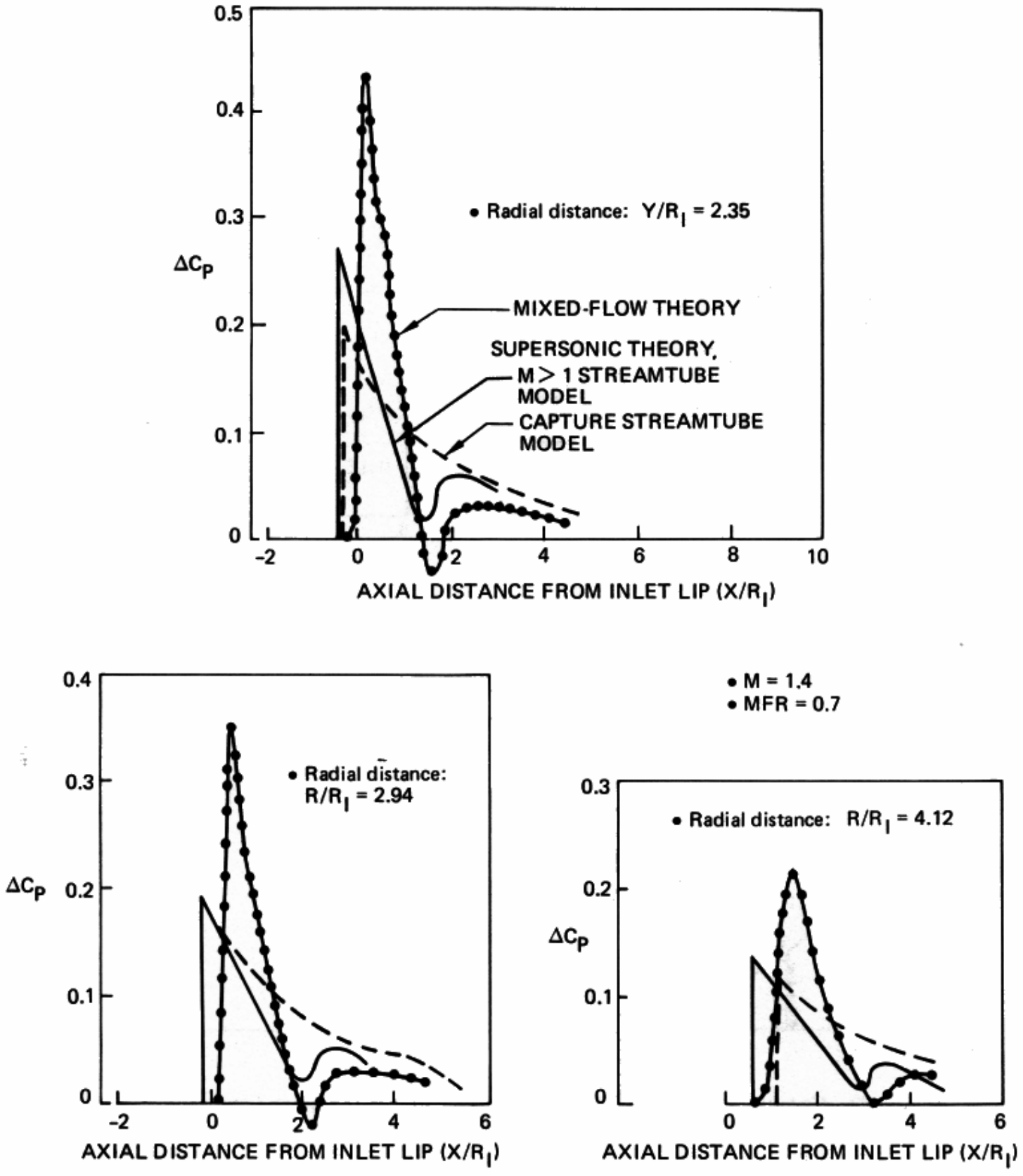

Figure 23. Comparison of Predicted Interference Pressures Around a Spilling Nacelle With a Mass-Flow of 0.7 Mach 1.4

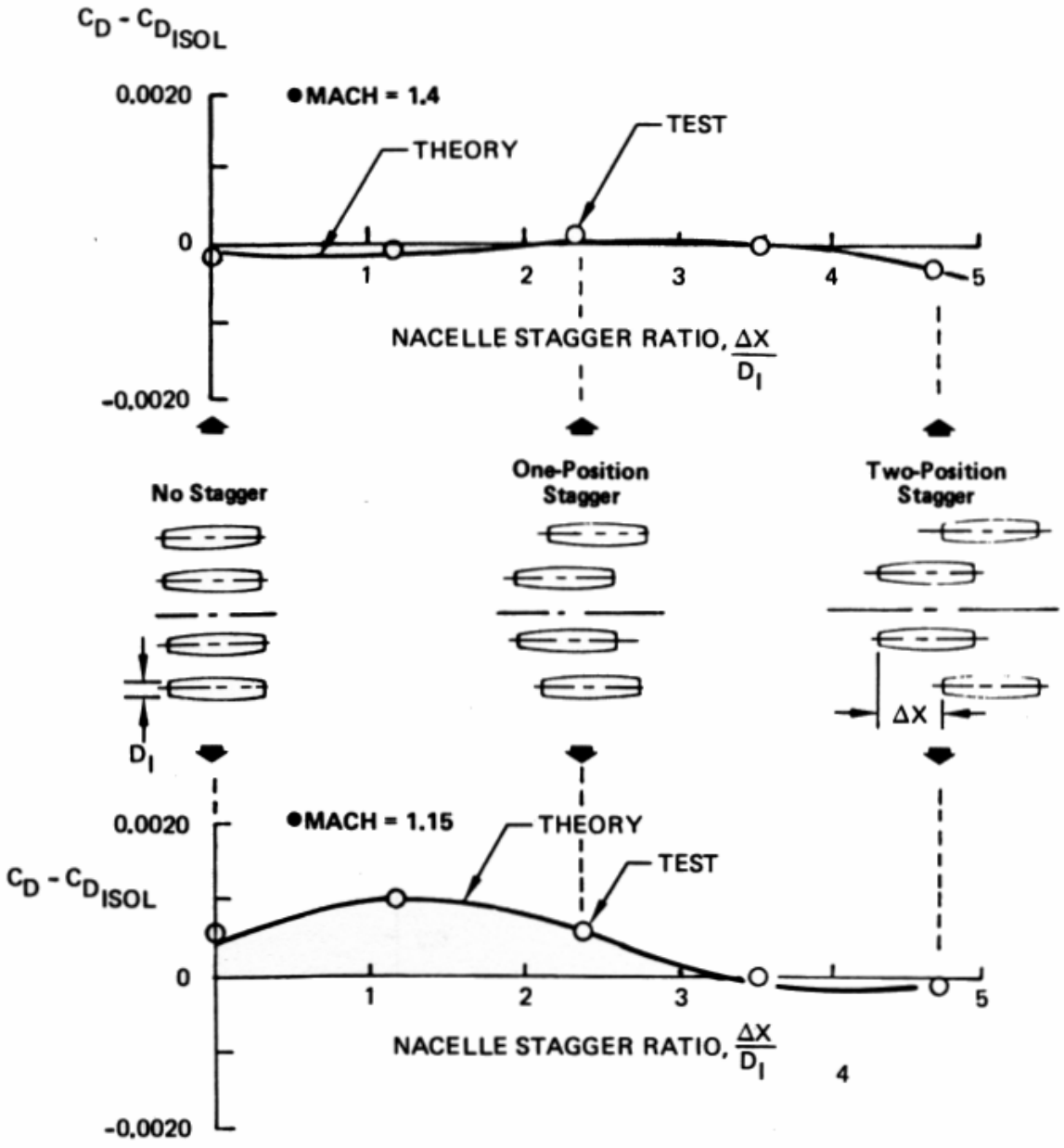

Figure 24. Drag Interference Between Nacelles at Zero Angle of Attack and a Mass Flow Ratio of Unity

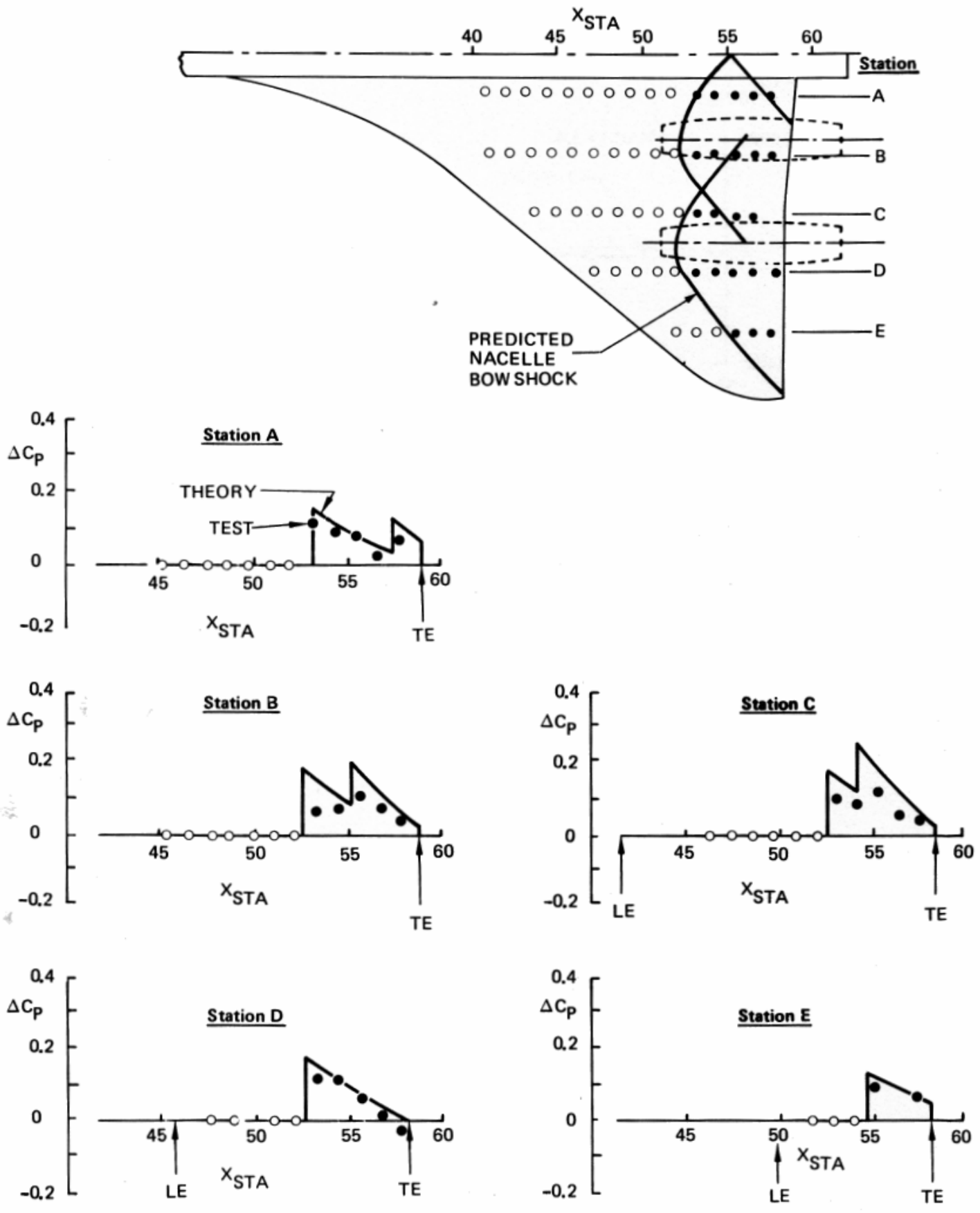

Figure 25. Effect of Nacelles Upon Wing Lower Surface Pressures at Zero Angle of Attack, Mach 1.4, and Mass Flow Ratio of Unity for an Aft Nacelle Location

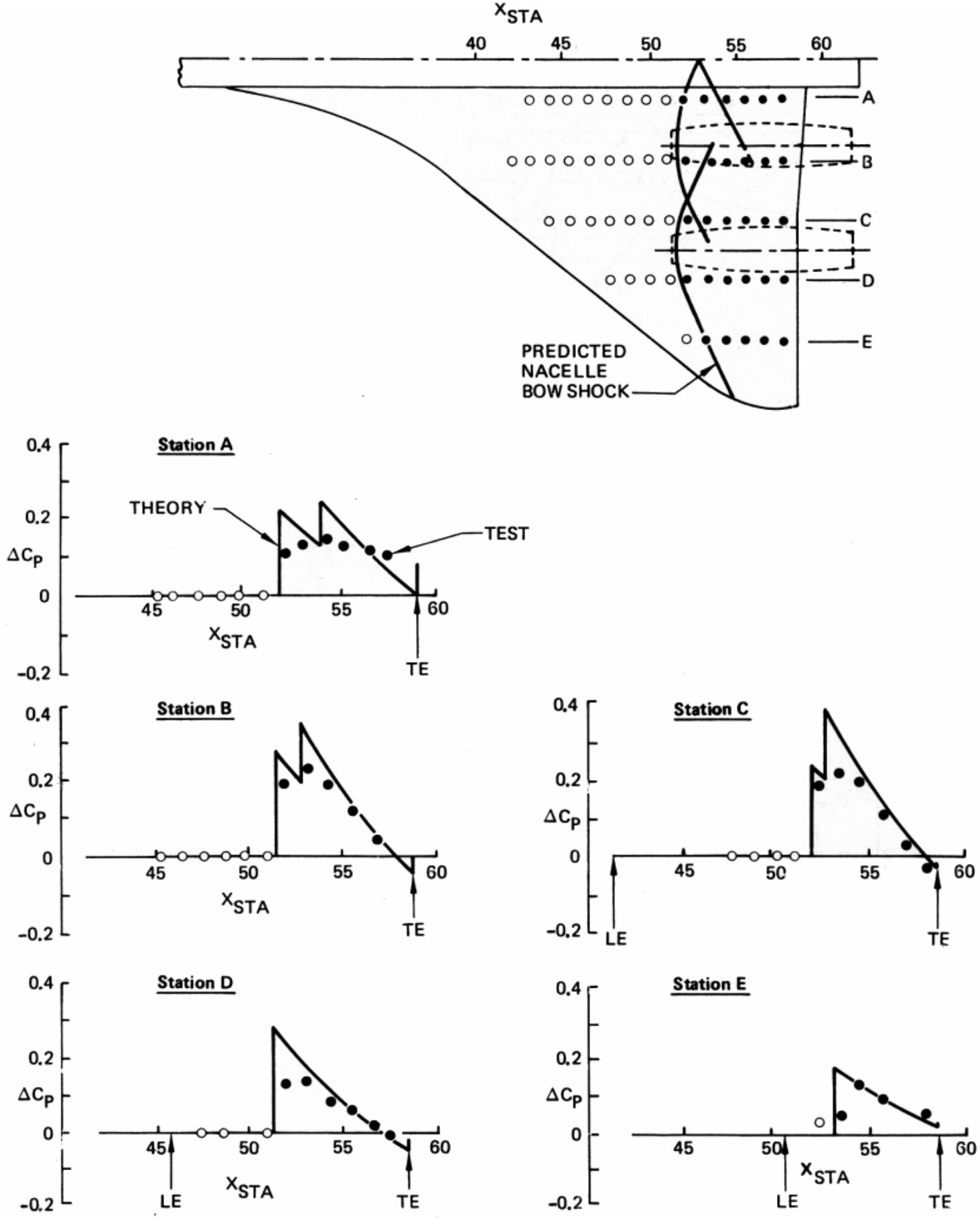

Figure 26. Effect of Nacelles Upon Wing Lower Surface Pressures at Zero Angle of Attack at Mach 1.15 and Mass Flow Ratio on Unity for an Aft Nacelle Location

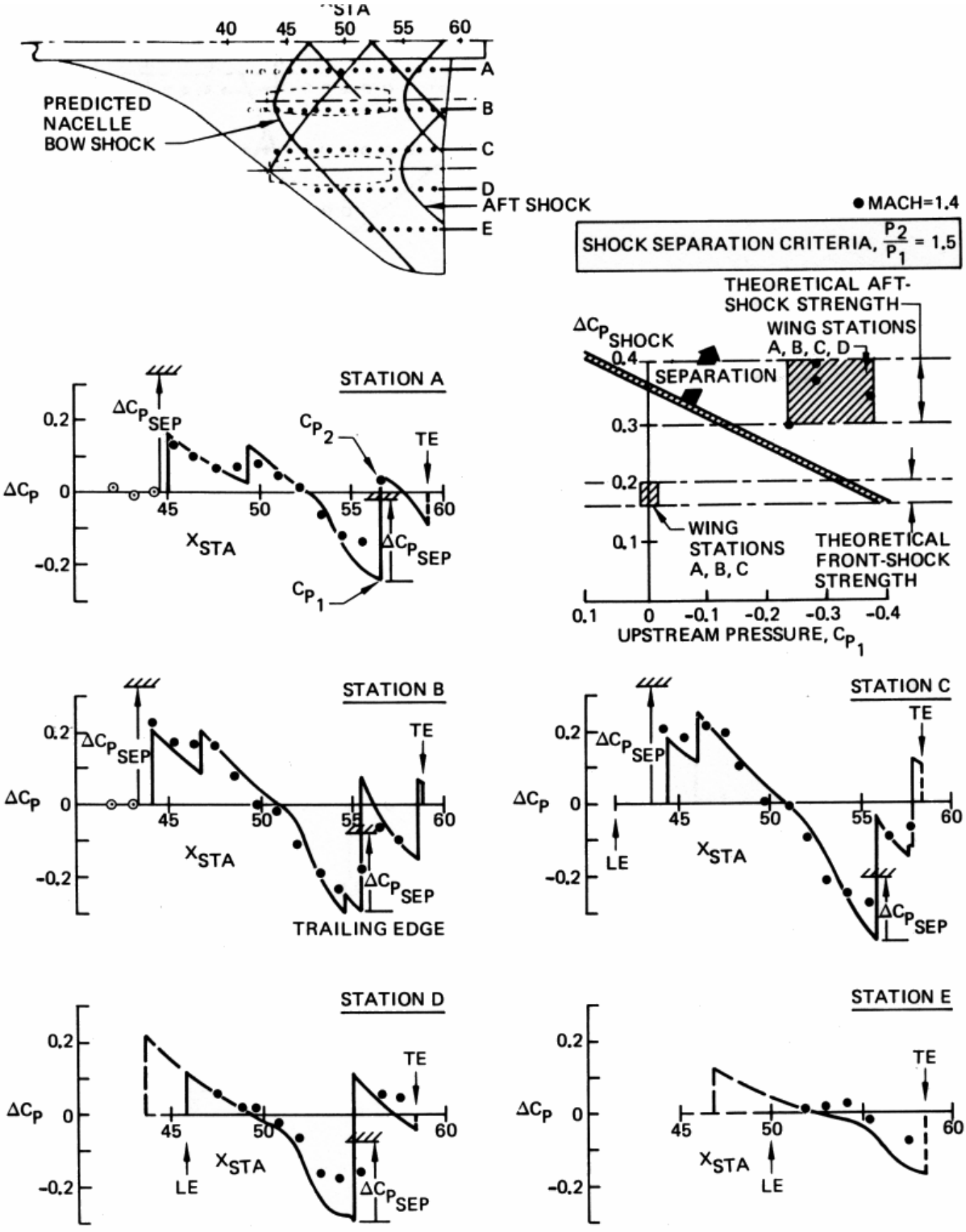

Figure 27. Effect of Nacelles Upon Wing Lower Surface Pressures at Zero Angle of Attack at Mach 1.4 and Mass Flow Ratio of Unity for a Forward Nacelle Location

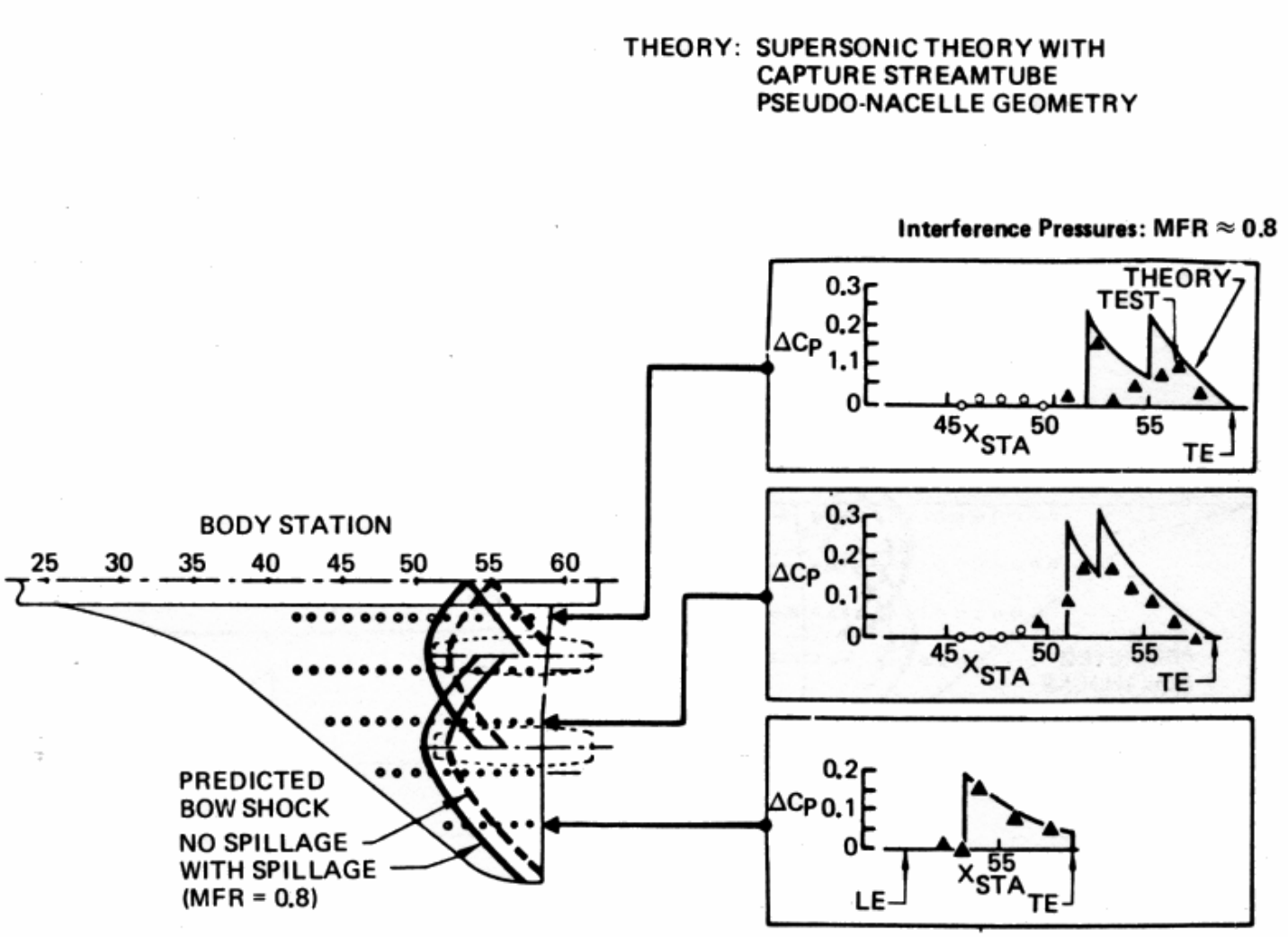

Figure 28. Effect of Normal-Shock Spillage on Isolated Nacelle Pressures and Wing Lower Surface Pressures at Mach 1.4, Zero Angle of Attack, and a Mass Flow Ratio of 0.8

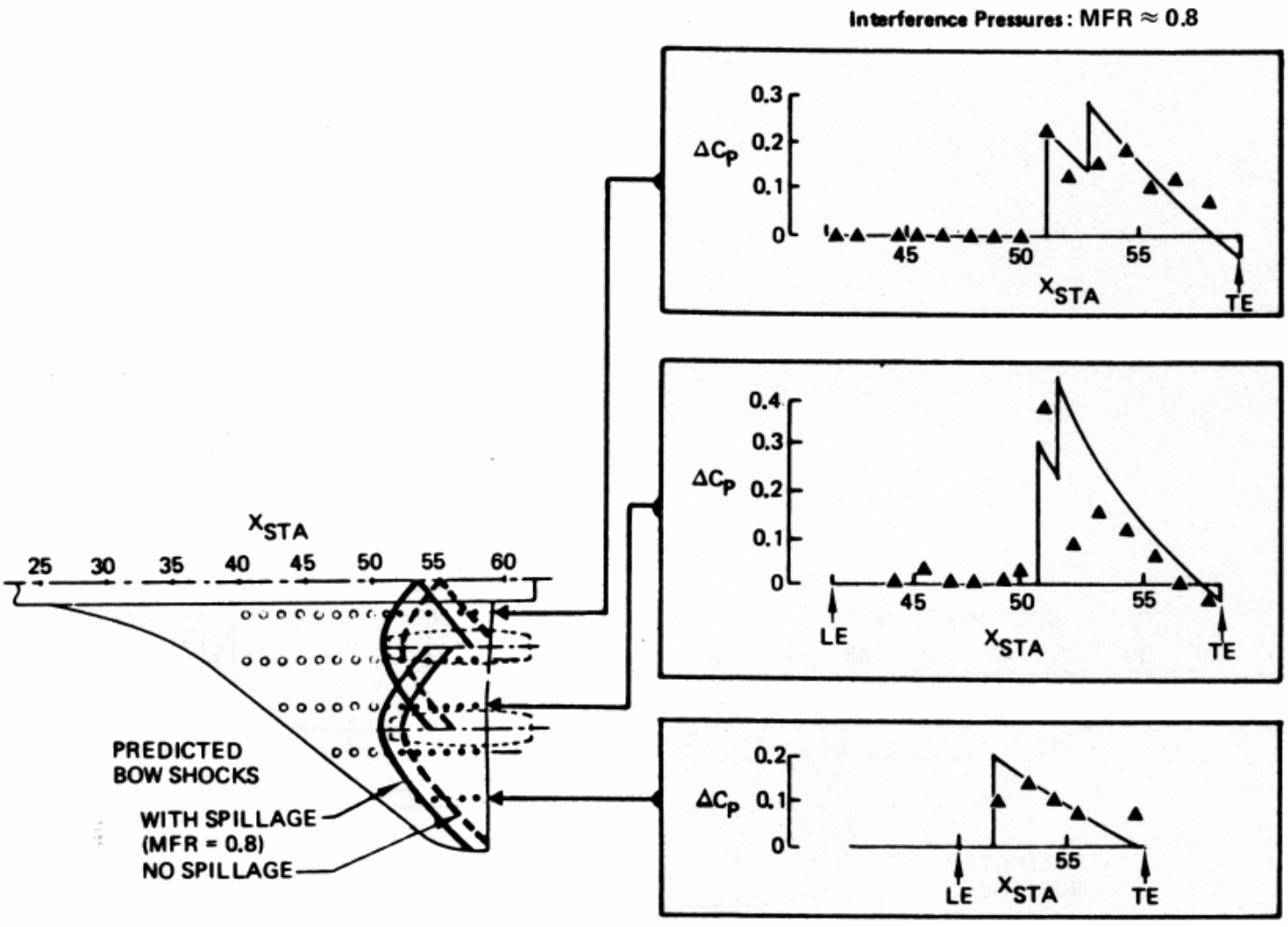

Figure 29. Effect of Normal-Shock Spillage on Isolated Nacelle Pressures and Wing Lower Surface Pressures at Mach 1.15, Zero Angle of Attack, and a Mass Flow Ratio of 0.8

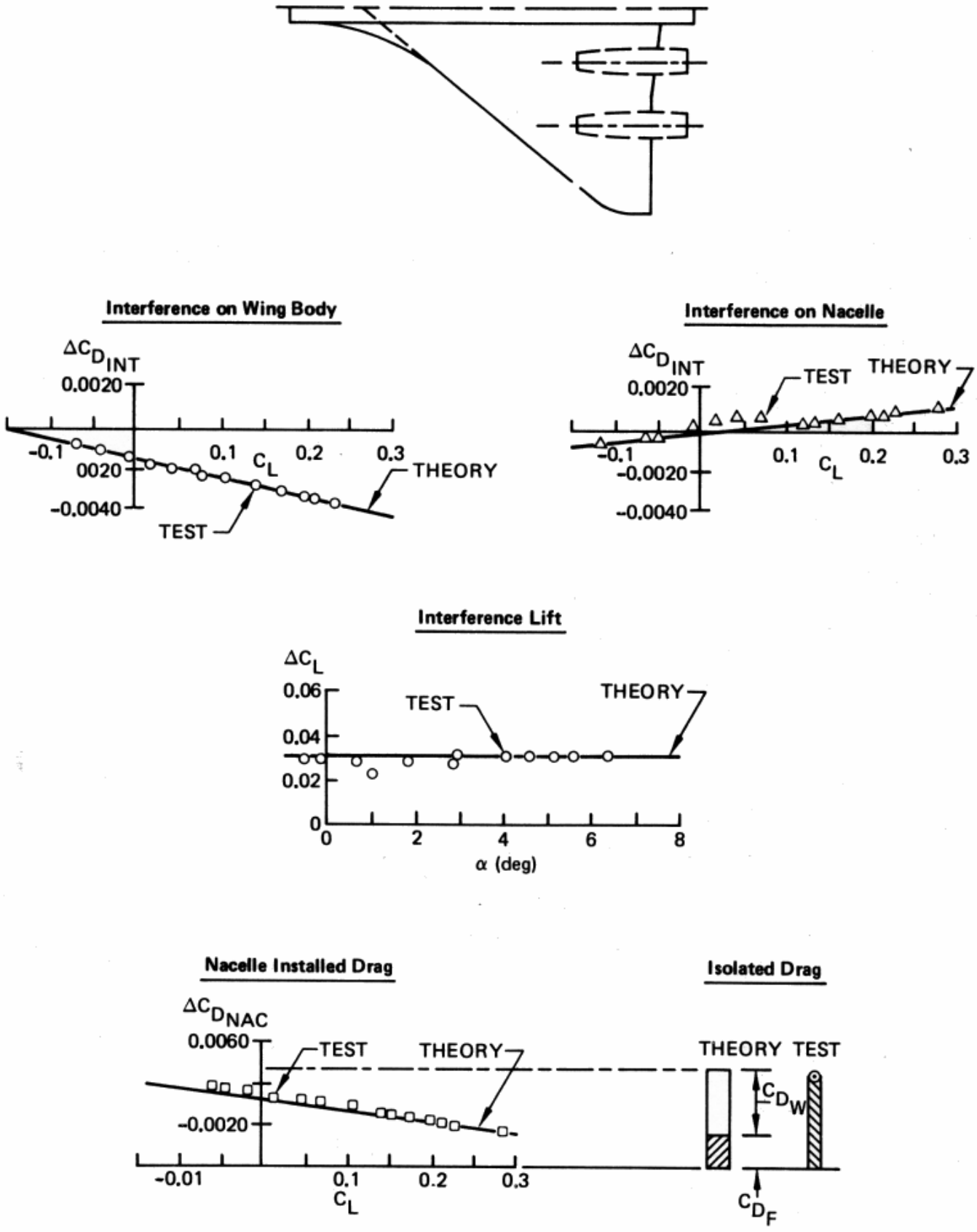

Figure 30. Installed Nacelle Drag for an Aft Nacelle Location at Mach 1.4 and Mass Flow Ratio of Unity

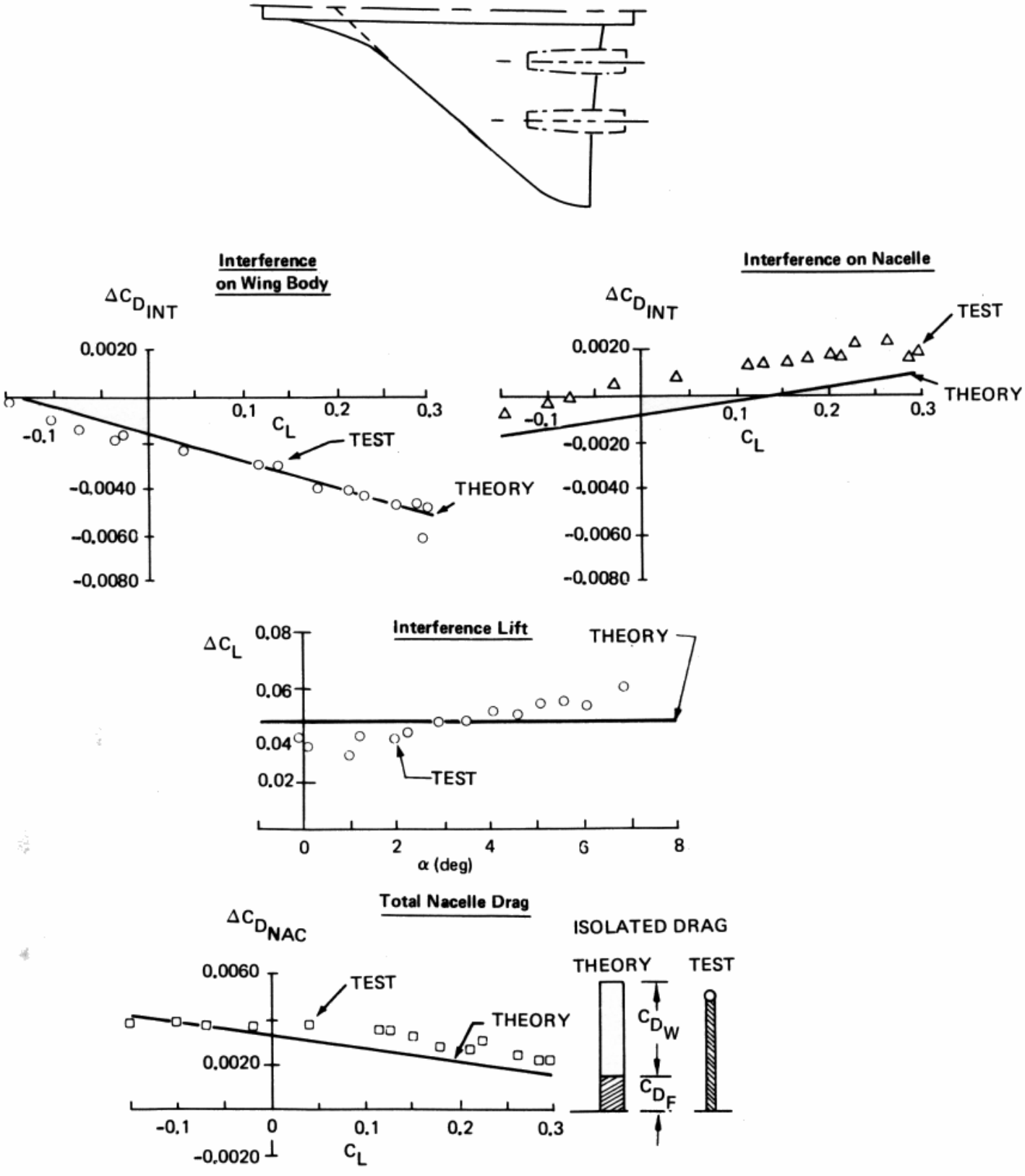

Figure 31. Installed Nacelle Drag for an Aft Nacelle Location at Mach 1.15 and Mass Flow Ratio of Unity

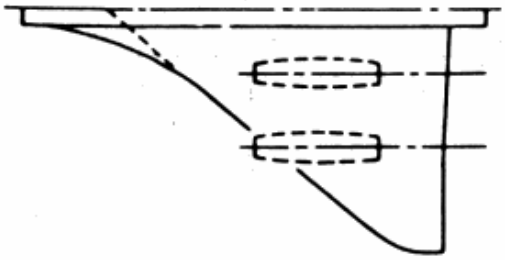

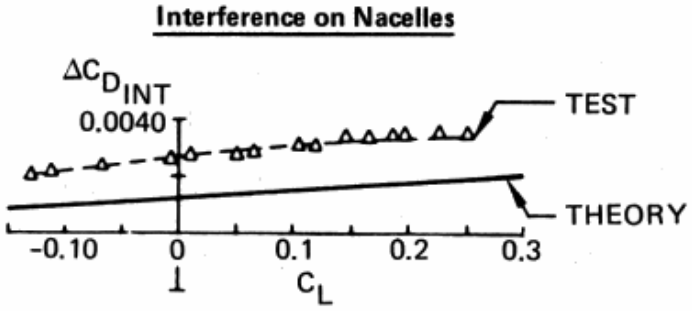

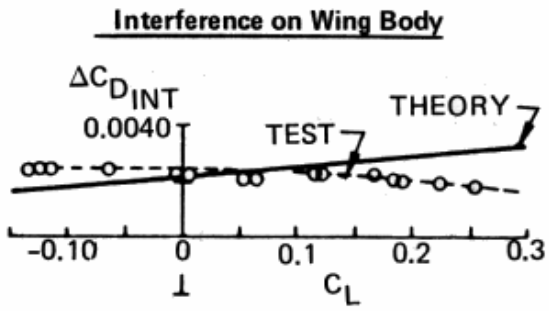

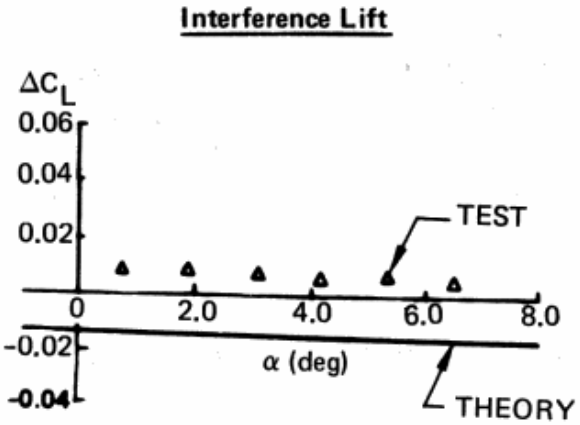

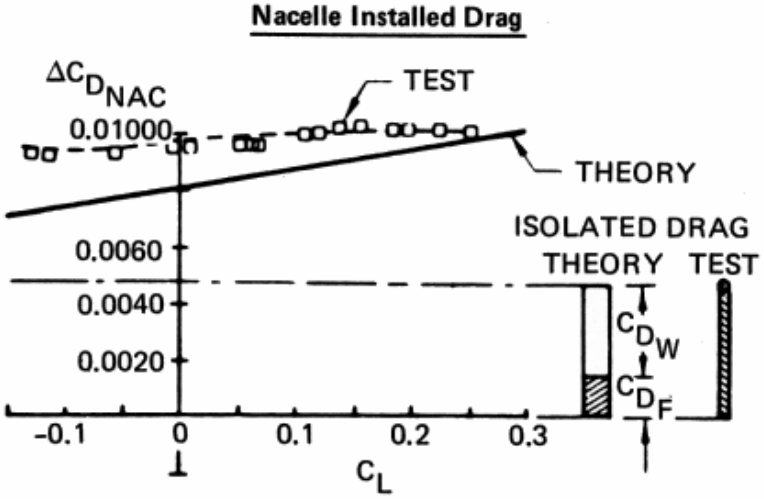

Figure 32. Installed Nacelle Drag for a Forward Nacelle Location at Mach 1.4 and Mass Flow Ratio of Unity

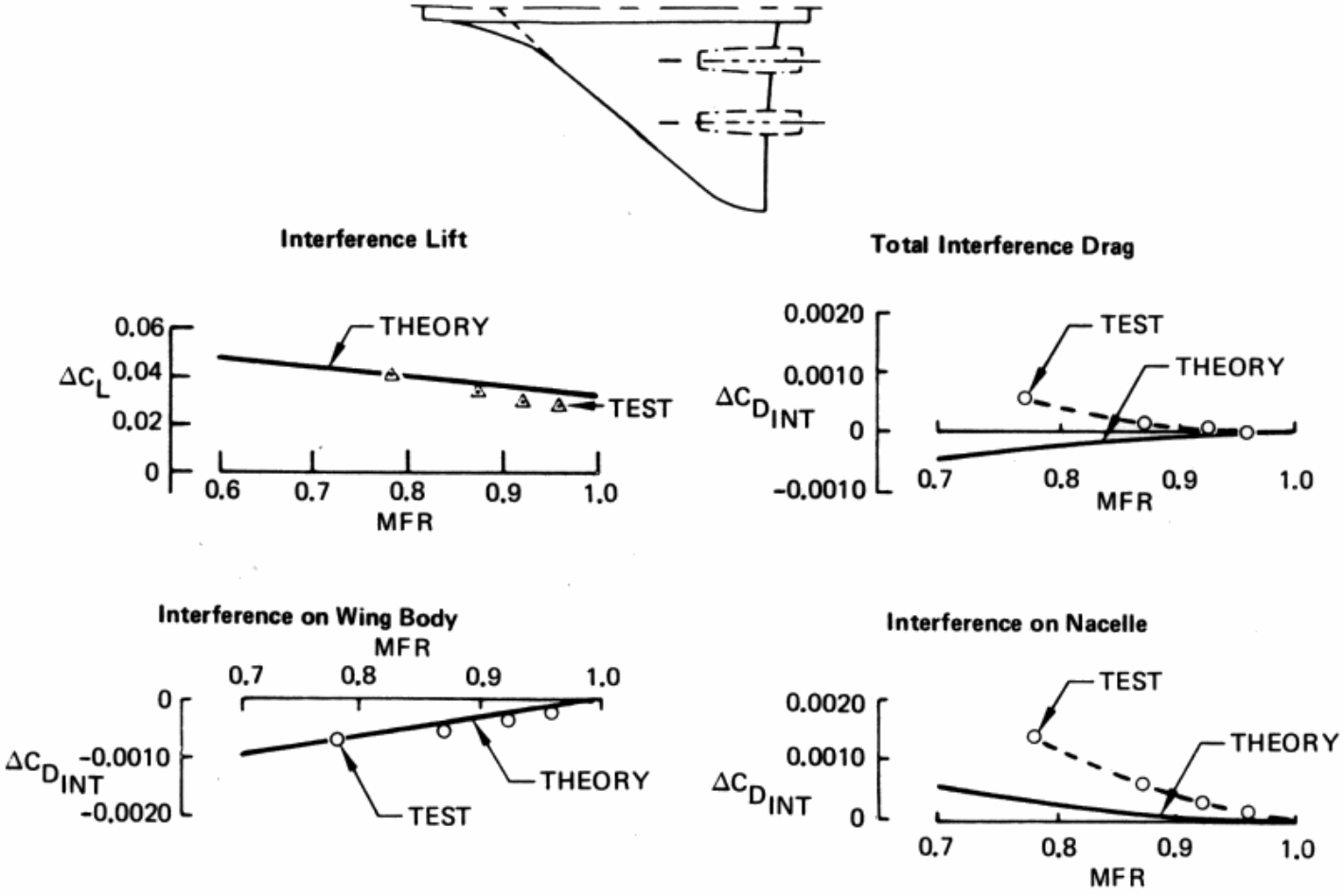

Figure 33. Effect of Normal-Shock Spillage on Interference Lift and Drag at Mach 1.4 and Zero Angle of Attack

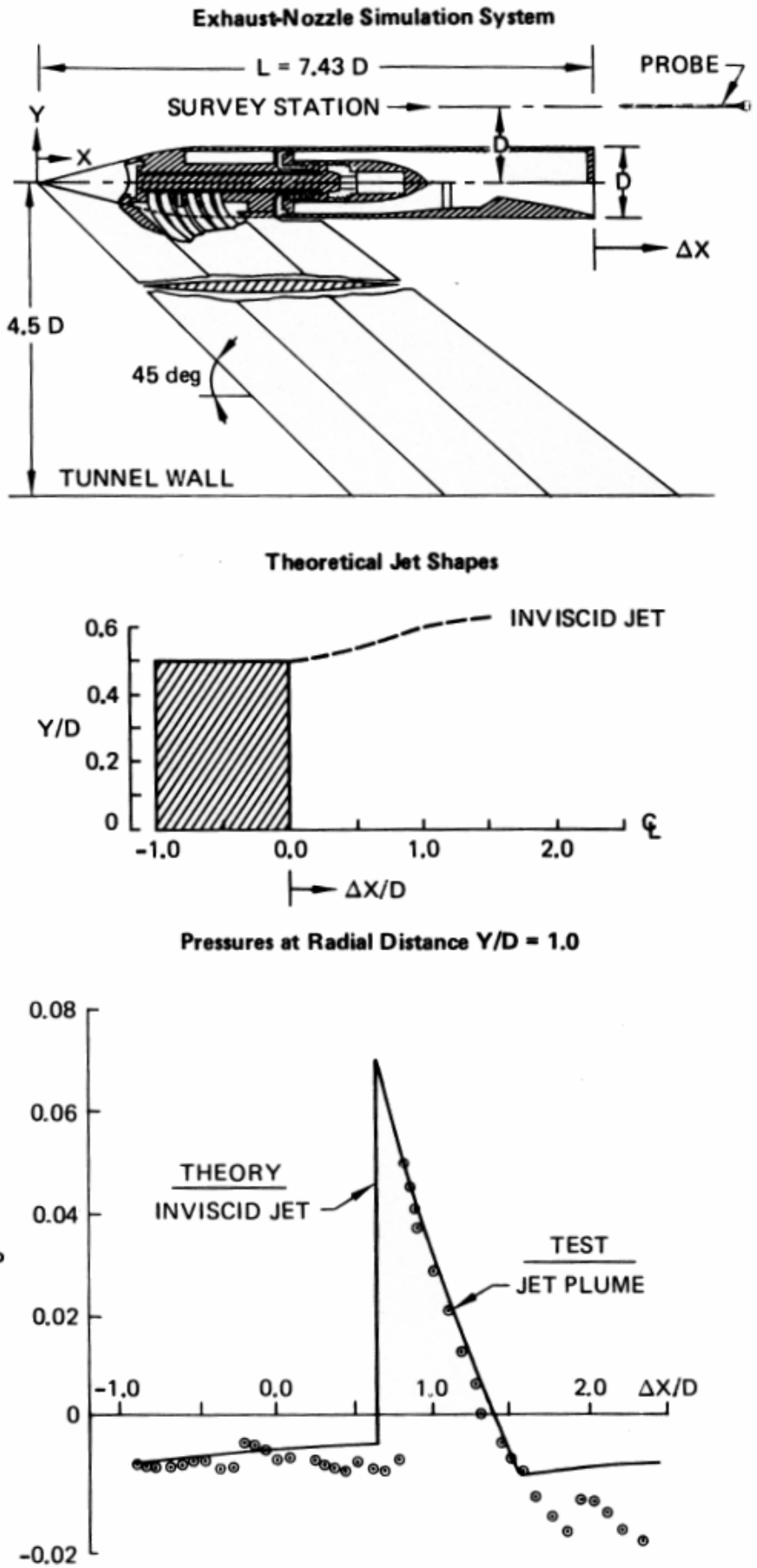

Figure 34. Comparison of Theoretical and Experimental Exhaust Jet Interference Pressures for an Underexpanded Jet (P_J/P_∞ = 1.093) at Mach 2.2

REFERENCES

1. Bencze, D. P.; Wind Tunnel Investigation of Nacelle-Airframe Interference at Mach Numbers of 0.90 to 1.4; NASA TMX-62, 489; 1976.

2. Bencze, D. P.; Wind Tunnel Investigation of Nacelle-Airframe Interference at Mach Numbers of 0.9 to 1.4; NASA TMX-73, 149 and 73, 088; 1976.

3. Bencze, D. P.; Experimental Evaluation of Nacelle-Airframe Interference Forces and Pressures at Mach Numbers of 0.9 to 1.4; NASA TMX-3321; March 1977.

4. Carmichael, R. L. and Woodward, F. A.; An Integrated Approach to the Analysis and Design of Wings and Wing-Body Combinations in Supersonic Flow; NASA TN D-3685, October 1966.

5. Woodward, F. A., Tinoco, E. N., and Larsen, J. W., Analysis and Design of Supersonic Wing-Body Combination, Including Flow Properties in the New Field; Part 1—Theory and Applications; NASA 31 CR-73106; 1967.

6. Tinoco, E. N., Johnson, F. T., and Freeman, L. M.; Application of a Higher Order Panel Method to Realistic Supersonic Configurations; AIAA Paper 79-0274; Journal of Aircraft, Vol. 17, No. 1, January 1980, pp. 38-44.

7. Middleton, W. D. and Lundry, J. L.; A System for Aerodynamic Design and Analysis of Supersonic Aircraft:

   Part 1—General Description and Theoretical Development; NASA CR-3351
   Part 2—User's Manual; NASA CR-3352
   Part 3—Computer Program Description; NASA CR-3353
   Part 4—Test Cases; NASA CR-3354, September 1980.

8. Peery, K. M. and Forester, C. K.; Numerical Simulation of Multi-Stream Nozzle Flows; AIAA Paper No. 79-1549; July 1979.

9. Kulfan, R. M. and Sigalla, A.; Real Flow Limitations in Supersonic Airplane Design; Journal of Aircraft, Vol.16, No. 10, pp. 645-658; October 1979.

10. Kulfan, R. M. and Blissell, W. A.; Analysis of Nacelle Transonic Interference Test Data, Section 4.0 of Advanced Concept Studies for Supersonic Vehicles; NASA CR-159244; May 1980.

11. Kulfan, R. M.; Final Report—Advanced Concept Studies for Supersonic Vehicles, Section 4.0; NASA CR—; April 1981.

12. Olstad, W. B.; Transonic-Wind-Tunnel Investigation of the Effects of Lip Bluntness and Shape on the Drag and Pressure Recovery of a Normal-Shock Nose Inlet in a Body of Revolution; NACA RM L56C28; July 1956.

13. Putnam, W. E. and Capone, F. J.; Experimental Determination of Equivalent Solid Bodies to Represent Jets Exhausting into a Mach 2.20 External Stream; NASA TN D-5553; December 1969.

ACKNOWLEDGMENT

This paper is based on work conducted for the Langley Research Center under NASA contract NAS1-14623 and also on work conducted for the Boeing Independent Research and Development program. The authors wish to thank Daniel P. Bencze for providing the data, model definitions, and photographs from the tests he conducted at NASA-Ames Research Center. The authors also wish to thank K. M. Peery, C. E. McFarland, L. J. Runyon, and W. D. Middleton for their efforts in providing the theoretical analyses and for many fruitful discussions.